REPORT DOCUMENTATION PAGE

Form Approved
OMB No. 0704-0188

1. AGENCY USE ONLY (Leave blank)	2. REPORT DATE	3. REPORT TYPE AND DATES COVERED
	01Dec94	Annual-from 15Oct93 to 14Oct94

4. TITLE AND SUBTITLE
Thrust-Induced Effects on a Pitching-Up Delta Wing Flow Field

5. FUNDING NUMBERS
F49620-93-I-0013

6. AUTHOR(S)
L. Lourenco, C. Shih, L. Van Dommelen and A. Krothapalli

7. PERFORMING ORGANIZATION NAME(S) AND ADDRESS(ES)
FAMU/FSU College of Engineering
Department of Mechanical Engineering (FAMU)
P.O. Box 2175, Tallahassee, FL 32316-2175

AFOSR-TR-96

0386

9. SPONSORING/MONITORING AGENCY NAME(S) AND ADDRESS(ES)
Air Force Office of Scientific Research
Division of Aerospace Sciences
Bolling AFB
Washington, DC 20332-6448

NA

10. SPONSORING/MONITORING AGENCY REPORT NUMBER
93-I-0013

11. SUPPLEMENTARY NOTES

12a. DISTRIBUTION/AVAILABILITY STATEMENT
Approved for public release,
distribution unlimited

19960624 257

13. ABSTRACT (Maximum 200 words)

The Thrust-induced effects on a pitching-up delta wing flow field are studied experimentally in a water towing tank facility. Previous report has shown that the jet has a signifigant effect in delaying the vortex breakdown over the delta wing. Strong asymmetric bursting of the leading edge vorticies can be induced by arranging the vectored jet in an assymmetric configuration. Extensive PIV measurements have been made to confirm these results. It is shown that the jet induces large accelerated flow along the vortex core which leads to more effective transportation of vorticity downstream. As a result, the primary vorticies are stabilized and strengthened. Also, a quasi-periodic variation of the instantaneous vortical structure on the cross flow plane is observed.

Concurrently, a numerical simulation technique based on the existing discrete vortex method is developed. A new grid-free "Vorticity Redistribution" technique is used to handle vorticity diffusion process. A test case involves unsteady seperation of flow over an impulsively started cylinder is studied using this new technique

14. SUBJECT TERMS	15. NUMBER OF PAGES
	88
	16. PRICE CODE

17. SECURITY CLASSIFICATION OF REPORT	18. SECURITY CLASSIFICATION OF THIS PAGE	19. SECURITY CLASSIFICATION OF ABSTRACT	20. LIMITATION OF ABSTRACT
UNCLASSIFIED	UNCLASSIFIED	UNCLASSIFIED	

DISCLAIMER NOTICE

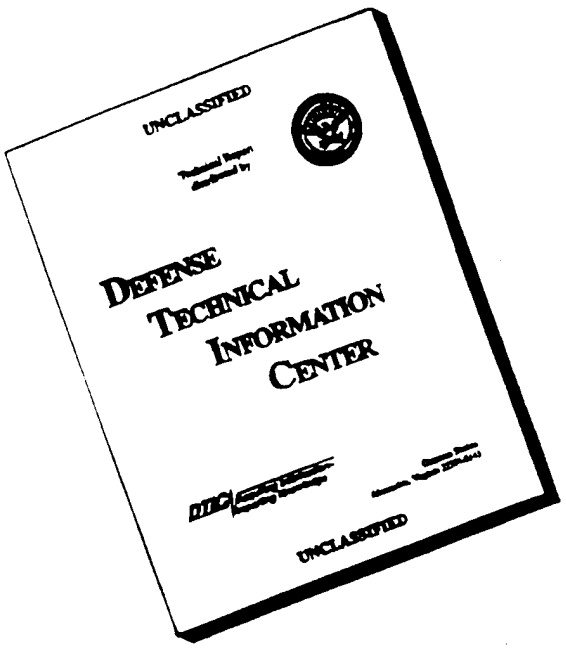

THIS DOCUMENT IS BEST QUALITY AVAILABLE. THE COPY FURNISHED TO DTIC CONTAINED A SIGNIFICANT NUMBER OF PAGES WHICH DO NOT REPRODUCE LEGIBLY.

THRUST-INDUCED EFFECTS ON A PITCHING-UP DELTA WING FLOW FIELD

by

L. Lourenco, C. Shih, L. Van Dommelen and A. Krothapalli

Department of Mechanical Engineering
Fluid Mechanics Research Laboratory
FAMU/FSU College of Engineering
Florida A&M University and Florida State University
Tallahassee, Florida 32316-2175

Contract # F49620-93-I-0013

Prepared for

Air Force Office of Scientific Research
Bolling Air Force Base, Washington DC 20332
Annual Report for the Period October 15, 1993 - November 1, 1994

TABLE OF CONTENTS

ABSTRACT

The thrust-induced effect on a pitching-up delta wing flow field is studied experimentally in a water towing tank facility. The delta wing has a leading edge sweep angle of 60° and a root chord of 13.0 cm. The Reynolds number, based on the free stream velocity ($U\infty$) and the root chord, is 9,800. Both static and dynamic (pitching) conditions are studied. The wing is pitched from 10° to 45° angle of attack with pitch rate varying from 0.04 to 0.4. The trailing edge vectored jet has a velocity range from 0.0 to 7.3 $U\infty$, and a control angle from 30° upward to 45° downward with respect to the wing. From dye flow visualization, it is shown that the downward control jet has a significant effect in delaying the vortex breakdown over the delta wing. Increasing the downward jet angle and the jet velocity will increase the effectiveness of the control. Strong asymmetric bursting of the leading edge vortices can be induced by arranging the vectored jet in an asymmetric configuration. Large delay of the vortex breakdown is consistently observed during transient pitching motion. From quantitative PIV study, it is shown that the jet induces large accelerating flow along the vortex core, it also strongly strengthens the primary vortical structure. Quasi-periodic variation of the instantaneous vortical structure on the cross flow plane is clearly observed.

Concurrently, a numerical simulation technique based on the existing discrete vortex method is developed. A new grid-free "Vorticity Redistribution" technique is used to handle vorticity diffusion process. A test case involves unsteady separation of flow over an impulsively started cylinder is studied using this new technique.

1. INTRODUCTION

Current interest in the development of highly maneuverable aircraft has prompted the extensive study of the flow past a delta wing. The most distinguishing feature of the delta wing flow field is the existence of a pair of well organized and highly energetic leading edge vortices (figure 1), formed at moderate angle of attack as a result of the flow separation along the sharp leading edge. Compared with the conventional two-dimensional airfoil, the occurrence of the delta wing stall is delayed to as high as 30° angle of attack.[1] Since the leading edge vortices induce large suction force on the delta wing surface, their existence can strongly enhance the overall performance of the aircraft. For example, vortices can account for as much as 30% of the total lift generated by delta wing aircraft operating at moderate angle of attack.[2] These advantages have been known for a long time, and leading edge vortex generating devices, such as leading edge extension (LEX) device, have been used successfully on some of the modern aircraft. Because of their importance to the aerodynamics of the aircraft, the leading edge vortices received significant amount of attention. Unfortunately, at high angle of attack, the vortices develop large scale instability that is characterized by the rapid deceleration and stagnation of the axial velocity along the vortex core, which leads to strong oscillation and total breakdown of the vortical structure. This phenomenon is commonly known as vortex breakdown, or vortex burst. After breakdown, the leading edge vortices lose their effectiveness to generate high lift force. Moreover, the strong oscillation associated with the vortex breakdown usually leads to the emergence of severe adverse effects, such as the wing rock. In order to achieve a controllable post stall maneuver, a fundamental understanding of the mechanism of the leading edge vortex flow field is necessary.

1.1 Physics of Leading Edge Vortex Flow over Delta Wing

Figure 2 is a sketch of the cross-sectional view of a leading edge vortex over a delta wing, with the corresponding distribution of circumferencial velocity and static pressure. The flow separates from the sharp leading edge of the delta wing, and the free shear layer rolls into a well organized vortical structure, commonly referred to as the primary vortex. Under the influence of the viscous effect, the thickness of the free shear layer increases as the flow moves downstream.[3] The vortical structure on the cross plane normal to the leading edge vortex core resembles a potential vortex with a viscous "subcore" at the center. Due to the influence of the delta wing surface, the flow in the cross plane is not axisymmetric in nature. Inside the primary vortex, the magnitude of the circumferencial velocity components increases towards the vortex axis, and reaches its maximum value at a point which is defined as the border of the subcore. Inside the subcore, the circumferencial velocity decreases drastically to zero at the vortex axis. The large velocity gradient inside the subcore signifies that the subcore is dominated by viscous effect. As for the static pressure, it decreases drastically towards the vortex core. As a result of this pressure distribution, the outer flow is entrained into the primary vortex, and is convected downstream along the vortex axis. The primary vortex grows in size and strength due to the constant feeding of vorticity from the leading edge separated shear layer. The swirl flow of the

primary vortex near the surface creates a boundary layer flow that moves outboard. As a result of the presence of an adverse pressure gradient along the cross flow plane, this outward flowing boundary layer separates from the delta wing surface. After separation the boundary layer rolls into a distinguishable vortical structure, which is commonly referred to as the secondary vortex. The secondary vortex is rotating in the opposite sense as compared with that of the primary vortex, both its size and strength are much smaller.

On the plane along the vortex axis, there exists a region with very large adverse pressure gradient. The axial velocity profile upstream of this region is of a jet-type, with the vortex core velocity accelerates, and overshoots the axial velocity component outside the core by a factor for up to three or more. After experiencing this large adverse pressure gradient, the centerline velocity along the vortex core decelerates drastically, in a form similar to that of the flow encounters a shock wave.[4] The centerline velocity decelerates to zero in about one to two upstream vortex core diameter, and is followed by a region of flow reversal. As a consequence, the vortex core is greatly expanded. The axial velocity now assumes a wake-type profile, and the flow field is exclusively turbulent.

1.2 Experimental Techniques and Observations

For decades, considerable emphasis has been placed on the understanding of the mechanism behind the vortex breakdown phenomenon, by means of numerical, experimental and theoretical studies. The majority of the early experimental studies involved the use of flow visualizations, along with force and surface pressure measurements. Flow visualization had been used extensively in both low and high speed experiments, as colored dye or smoke were used to track the vortex breakdown process. Most of the qualitative information concerning the vortex breakdown process, including the onset, the location and the type of vortex breakdown, is acquired through the use of the flow visualization technique. However, its effectiveness is limited when quantitative information of the flow field is sought.

The followings are some of the common features for steady flow observed through flow visualization:

1) When the delta wing is set at a moderate angle of attack, two distinct leading edge vortices appear, and the vortex breakdown first appears downstream of the trailing edge, which is a result of the sudden expansion of the flow leaving the trailing edge. The vortex breakdown is characterized by large oscillation and quick dispersion of the dye.

2) When the angle of attack is further increased, first the vortex breakdown location moves quickly upstream towards the apex, then, when the angle of attack is beyond some certain value, the propagation of the vortex breakdown location slows down.

3) When the angle of attack is increased to very high value, the vortex breakdown location moves all the way to the apex, no distinguishable vortex core can be seen, and total breakdown occurs thereafter.

4) Two types of vortex breakdown are observed (Figure 3)[5]: the spiral-type vortex breakdown and the bubble-type vortex breakdown. For the spiral-type breakdown, the dye assumes a spiral shape and rotates about the vortex axis in the same sense as does fluid in the upstream vortex; for the bubble-type breakdown, the dye assumes a shape that is similar to a body of revolution placed in the flow.

Since leading edge vortex flow about the delta wing is three-dimensional and the vortex breakdown process is extremely sensitive to small disturbance, the use of intrusive technique such as conventional pressure probes or hot-wires will disturb the flow field, and make the measurements highly unreliable. Recently, new and more powerful non-intrusive experimental techniques, such as Laser Doppler Anamometry (LDA) and Particle Image Velocimetry (PIV) have been broadly utilized, resulting in the drastic improvement in the understanding of the leading edge vortex flow. LDA is able to provide continuous information at one given point. PIV technique is able to provide instantaneous whole-field two-dimensional velocity information with very fine spatial resolution. Both LDA and PIV are non-intrusive techniques, this makes them ideal for measuring the flow over the delta wing. The delta wing flow field is a vortex dominant high shear flow, this requires high spatial resolution for the flow field. On the other hand, instantaneous flow field information is necessary in order to understand the dynamic effect of pitching on vortex breakdown. Considering all aspects, it is especially desirable to use the instantaneous whole-field measurement technique such as PIV to study the delta wing flow field.

1.3 Aspects of Vortex Breakdown

1.3.1 Geometry

The effect of delta wing geometry on vortex breakdown had been the goal of intensive study in the early years, and it had been known for a long time that the geometry greatly affects the aerodynamics of the wing. Erickson [6] gave a detailed account of the influence of leading edge sweep angle on the vortex breakdown. He pointed out that, when the other conditions were held the same, the larger the leading edge sweep angle, the closer to the trailing edge the breakdown location would be. Wentz and Kolhman [7] made thorough parametric studies of the delta wing leading edge sweep angle φ range from 45° to 85°. They found out that for $\varphi > 75°$, the breakdown process became independent of the sweep angle. Kegelman and Roos [8], and Panton [9] studied the effect of different leading edge shapes on vortex breakdown.

Apart from geometrical consideration, the effect of the Reynolds number on vortex breakdown in the low speed range was studied by Lowson[10] in a subsonic wind tunnel. The result of the breakdown process at supersonic flow was published by Craven and Alexander[11], and by Monnerie and Werlé [12].

1.3.2 Adverse Pressure Gradient

Progress in the theoretical descriptions for vortex breakdown had been reviewed by Hall[13], and more recently by Leibovich [4]. Various theories arise as to what plays a decisive role in the vortex breakdown process, and what is the mechanism behind the vortex breakdown phenomenon. Most people agree that the adverse pressure gradient along the vortex core plays an important role in the vortex breakdown process. The stream-wise pressure gradient on the delta wing surface is inevitably an adverse one, due to the existence of its trailing edge. The magnitude of the adverse pressure gradient depends on the delta wing geometry [14], such as the angle of attack and the leading edge sweep angle. The higher the angle of attack or the smaller the leading edge sweep angle, the more severe the adverse pressure gradient is. The existence of the adverse pressure gradient along the vortex core causes the axial velocity to decelerate,

become stagnate and eventually reverse. Thus an increase in the magnitude of the adverse pressure gradient results in earlier breakdown of the leading edge vortex.

1.3.3 Swirl Angle and Azimuthal Vorticity

As Gursul et al.[14] suggested, two parameters played important role in deciding the vortex breakdown location. The first parameter was the external pressure gradient outside the vortex core, and the second was the swirl angle which is defined as $\phi=\tan^{-1}(v/u)$, where v and u are the swirl velocity component and the axial velocity component, respectively. They argued that small external pressure gradient could be amplified along the vortex core, thus made the adverse pressure gradient inside the vortex core more severe. When the swirl angle was increased, the leading edge vortex breakdown location moved upstream. The swirl angle measurements over the delta wing and the vortex tube suggested that there existed a critical value for the swirl angle[15], which was larger than 40°. The breakdown would occur when the swirl angle exceeded this critical value. For a leading edge vortex, the swirl angle was also related to the delta wing geometry, such as the leading edge sweep angle and the delta wing angle of attack.

On the other hand, in their theoretical model Brown and Lopez [16] place emphasis on the crucial role of both the velocity and vorticity helical angles. They suggested that the onset of the negative azimuthal vorticity was a necessary condition for the onset of vortex breakdown. Later, in their PIV study of the flow field along the vortex core, Towfighi et al.[17] also showed that the sign of the azimuthal vorticity switched at the onset of vortex breakdown. That is, upstream of vortex breakdown, the vorticity was relatively distributed and located adjacent to the wing surface. If this vorticity is defined as positive, then after the vortex breakdown, the relatively concentrated vorticity that was close to the surface became negative. This switch in sign of the azimuthal vorticity had also been observed experimentally by Rockwell et al.[18] and numerically by Visbal [19].

1.3.4 Stability Analysis

A number of the theoretical works involve stability analysis of the delta wing flow field. Gad-el-Hak and Blackwelder [20] first observed that, in the water tank experiment, the vortex sheet generated at the leading edge of the delta wing rolls into discrete vortices which undergo a paring process. This instability and pairing process is similar to the instability and vortex pairing process that experienced by a two-dimensional free shear layer as described by Brown and Roshko[21]. As Rediniotis[22] recently pointed out, von-Karman type periodic shedding was observed over delta wing at high angle of attack. Periodic vortex shedding often induces significant asymmetry on the pressure distribution over the delta wing surface. This couples with the motion of the aircraft will lead to catastrophic effects such as wingrock. Payne et al.[23] also observed the instability in the vortex sheet which formed the primary vortex, again the growth of the secondary structure was related to the classical Kelvin-Helmhotz Type instability. In his paper, Lowson [24] reported two types of instability, the first type was the Kelvin-Helmhotz Type instability of the shear layer leaving the leading edge of the delta wing, as described by Gad-el-Hak. The second type was the locally streamwise instability of the feeding vortex sheet that gave rise to steady vortex cell structure within the vortex core.

As Leibovich [4] pointed out, virtually all of the theoretical efforts adopted the idea that the nonaxisymmetric effects were incidental, and the dominant mechanism of vortex breakdown was

axisymmetric. This idea was based on two arguments. The first argument was that, the contribution of the axisymmetric component was significantly larger than the those of the nonaxisymmetric components. The second argument was that the Navier-Stokes Equation might admit exact, steady, axisymmetric vortex breakdown solutions. Adopting this idea, Leibovich made further analysis and suggested that vortex breakdown might be caused by the expansion and eventual instability of the axisymmetric wave, which was caused by the adverse pressure gradient along the vortex axis.

1.3.5 Dynamic Pitching

In recent years, more attention has been focused on the study of the dynamic behavior of the delta wing, as due to the fact that swift pitching motion is a basic requirement for a highly maneuverable aircraft. The dynamic conditions considered in these studies include single ramp-typed pitching-up or pitching-down motion, sinusoidal motion, and continuous ramp-type pitching motion. Most of the experimental studies were carried out using flow visualization technique. It was found out that the swift pitching motion always resulted in significant departure from the quasi-steady state. Large delay of the vortex breakdown process was consistently observed in the experiments. As Thompson et al.[25] pointed out that, compared with the static angle of attack case, the ramp-type pitching motion delayed the vortex breakdown location much further downstream. In addition, the higher the pitch rate, the more effective this delay became. The delay of the vortex breakdown also reflects the aerodynamics of the delta wing. As Jarrah observed, [26] there was an overshoot of the curve of the lift coefficient versus the angle of attack. He attributed this overshoot to the fact that the propagation of the vortex breakdown location had been delayed. He further pointed out that with the increase of the aspect ratio of the delta wing, this overshoot became more prominent. He noticed that before the breakdown points appeared at the trailing edge, the lift coefficient of the pitching delta wing coincided with those corresponding to the stationary wing. Magness et al.[27], Lemay et al.[28] showed that during the pitching motion of the 75° sweep angle delta wing, the propagating speed of the vortex breakdown location was nearly constant, and could be normalized to a single value by the reduced frequency or the reduced pitching rate. Rediniotis et al.[29] pointed out that the dynamic development of the flow lagged behind the corresponding quasi-steady pattern during the pitching motion. They further suggested that the breakdown of axial velocity might precede axial vorticity breakdown.

1.4 Control of the Vortex Breakdown

Vortex breakdown always induces adverse effects which seriously affect the stability and maneuverability of the aircraft. In order to effectively utilize the leading edge vortex flow, it is important to control the vortex breakdown process. If vortex breakdown can be delayed to a higher angle of attack, the resulting stablized vortex flow would significantly improve the performance of the aircraft. Extensive work on vortex control had been done by Erickson[30] in both water channel and wind tunnel facilities using spanwise blowing technique. Spanwise blowing induced spanwise flow gradient similar to those naturally happened on highly-swept wings, and effectively delayed the vortex breakdown to a higher angle of attack. Werlé[31] also demonstrated the effective control of the separated flow regions by lateral blowing. Recent work

by Erickson[32] on wing/leading edge extension configuration showed significant aerodynamic benefits due to lateral blowing at moderate to high angles of attack. Control of vortices by steady blowing along or at the leading edge had been studied by Bradley et al.[33], Shi et al.[34] and Wood et al.[35], as substantial changes in the magnitudes of the surface suction pressure and normal force were attained. Those were believed to be due to a change in the strength of the leading edge vortices, which caused the reduction of the swirl angle. Unsteady injection had also been studied, it was found out that periodic blowing/suction applied normal to the leading edge of the delta wing significantly enhanced the coherence of the vortical structure in the leading edge free shear layer. On the other hand, transient suction along the vortex axis also delayed the onset of the vortex breakdown. Recently, Gu et al.[36] compared the steady and unsteady blowing technique, and found out that alternating blowing/suction produced the largest delay of vortex breakdown. In all these leading edge blowing cases, the delay achieved is relatively steady. Srinivas et al.[37] recently studied the active control of vortex breakdown over delta wing. They suggested that the pressure fluctuation induced by the helical mode instability of vortex breakdown could be used to control the vortex breakdown process.

The maneuverability of modern fighter aircraft is achieved primarily through the use of leading or trailing edge devices. Because of the flight condition, these devices are always exposed to unsteady flow that limits their effectiveness. In addition, the response of these mechanical devices is not quick enough in high speed and high angle of attack condition. One alternative for these control devices is the integration of aircraft propulsive and lift system. As Hagedon and Ruden [38] demonstrated that a thin jet sheet deflected from the airfoil's trailing edge could be used in place of the mechanical flap to achieve high lift coefficient. The jet flap, as the configuration is called, offers a number of advantages in both low and high speed flight regimes.

The thrust-induced effect on the aerodynamics of the Short Take-Off and Landing (STOL) fighter configuration had been studied intensively in the past.[39,40,41] The benefits associated with such aero-propulsion integration include:

1) Increased lift attributed to induced aerodynamics created by the nozzle exhaust flow near the trailing edge.

2) Increased instantaneous maneuvering capability with a vectoring exhaust jet.

3) Improved cruise performance due to reduced aftbody drag.

4) Reduced radar reflection cross section, infrared signature, and noise.

Since propulsion can significantly affect the wing's lift, drag, and pitching moment coefficients, the wing aerodynamics and the propulsion system performance are closely linked. As shown in figure 4, the contribution of the jet induced effect can be as large as the jet thrust component in the lift direction, and a significant drag reduction is also achieved. These can be attributed to the favorable interaction between the jet and the wing flow field.

The studies mentioned above clearly show that properly designed integration of the aero/propulsion system will greatly improve the performance of the aircraft. However, all of these studies are oriented at studying high lift devices for two dimensional wing, and are confined to low angle of attack ($< 20°$) cases. As the effect of trailing edge vectored jet on the leading edge vortex flow of the delta wing is concerned, very little information is available.

1.5 Objective

Based on the previous discussion, the following objectives is proposed:

1) to study the dynamic (pitching) effect on the leading edge vortex flow of the delta wing;

2) to investigate the effect of trailing edge vectored jet on the leading edge vortex flow of the delta wing, at static angle of attack and during transient pitching;

3) to investigate the effect of distributed vectored jet on the dynamic behavior of the delta wing.

The focus of the study is to understand the thrust induced effect on the leading edge vortex flow structure.

In order to achieve the above stated objectives, it is necessary to describe the flow field in terms of the unsteady and three-dimensional vortical structure. With the development of Particle Image Velocimetry technique in our laboratory, it is now possible to obtain instantaneous whole field velocity and vorticity information. PIV is a two-dimensional measurement technique which is able to provide instantaneous velocity information with high spatial resolution, and here it is selected as the means to study the quantitative behavior of the flow field.

The delta wing model is specially designed to have two rectangular vectored nozzles mounted at its trailing edge, in order to simulate the aero/propulsion integration. Different nozzle configurations are used to provide different jet vectored angles.

The investigation is carried out in a water towing tank facility. The low speed experiment is aimed to understand the basic flow physics. Conventional dye flow visualizations will be carried out to test a wide range of parameters. These will be followed by PIV investigations on selected cases.

The delta wing model has a leading edge sweep angle of 60° and a root chord of 13.0 cm. The Reynolds number, based on the free stream velocity ($U\infty$) and the root chord, is 9,800. For the steady case, the angle of attack varies from 10° to 35°. For the dynamic pitching case, the delta wing is pitched from 10° to 45°, and the non-dimensionalized pitch rate varies from 0.043 to 0.39. The vectored jet angle can be varied from 30° upward to 45° downward (with respect to the delta wing surface), and the jet velocity can be varied from 0 to 7.3 $U\infty$.

2. EXPERIMENTAL SETUP

2.1 Water Towing Tank Facility

The experiments are performed using the water towing tank facility (figure 5) in the Fluid Mechanics Research Laboratory (FMRL). The water towing tank is made of 12.7 mm thick glass plate, with dimensions of 3.6m in length and 0.55 × 0.42 m in cross section. The water tank is supported by steel-frame structure, with rubber pads being used to absorb the vibrations from the ground. A computer-interfaced Anorail™-5 Linear motor (Model 3911, single slide) is used to drive the towing carriage. The linear motor is mounted face down on top of the water tank, and is supported by the steel frame. This linear motor employs closed-loop DC servo position control, the position feedback is provided by an incremental linear optical encoder. This allows for fine control of the position. The motor controller is linked to a host computer, an IBM PS/2 model 70 system. The commands, such as travel speed, acceleration, travel distance and home, are downloaded to the controller through RS232 interface. The maximum travel distance in the present experimental condition is about 250 cm, and the maximum travel speed is about 30 cm/s.

There are three moving platforms in the system. The first platform, used for model mounting, is directly fixed to the slide of the linear motor. The other two platforms, one for mounting the image recording system and the other for the rotating mirror used to create the multiple pulsed laser illumination, are mounted on two separate rails and are synchronized with the motion of the linear motor through a gear/belt system.

2.2 Particle Image Velocimetry (PIV) System

2.2.1 Advantages of the PIV Technique

Particle Image Velocimetry is a non-intrusive experimental technique which is able to provide instantaneous two dimensional whole field velocity information. It belongs to a broader group of Pulsed Light Velocimetry technique. By recording the multiple exposed images of the seeding particles, PIV images contain the information of the displacement of the illuminated particle images between successive exposures. The local velocity is determined by the equation $u=\Delta x/\Delta t$, where Δx is the displacement between two consecutive exposures of the same particle image, and Δt is the corresponding time. The multiple particle images are recorded on optical recording media, such as photographic film, video, or holographic film. An overview of Particle Image Velocimetry is given by Adrian [42] and Lourenco et al..[43]

Conventional flow field measurement techniques can be classified into two groups: intrusive and non-intrusive. Intrusive technique includes hot wire measurement and pitot tube measurement. They are both single point measurement techniques, that is, they only able to provide instantaneous information on one given point. No matter how small they are made, their presence will disturb the neighboring flow structure. Laser Doppler Anemometry (LDA) and Particle Image Velocimetry are both non-intrusive techniques. But LDA also has the draw back of only being able to measure one given point at a time. As the delta wing flow field is concerned, first the leading edge vortex is extremely sensitive to small disturbance, that makes any use of probe or hot wire near the vortex core unacceptable, and, when dealing with unsteady

flow (such as pitching motion of the delta wing), the effectiveness of LDA becomes limited. PIV technique is able to provide whole field instantaneous velocity information with good spatial resolution, and is the better available technique in the study of unsteady flow, or large scale shear flow, as is dominant in the delta wing flow field.

2.2.2 Principle Of the PIV Technique

The detailed description of the technique of PIV is given by Adrian and Lourenco. et al.. Here is a brief description of the principle of this technique used in our experiment: A continuous Argon laser (model # 171-00) is selected as the coherent light source. A 24-faceted rotating mirror placed in front of the laser sweeps the laser beam into pulsed laser sheets, and projects them to the plane of interest. Within the illuminated plane, the flow is made visible by seeding tiny silver-coated tracer particles into the water. The diffraction of the light from these particles is very strong, and thus their images are able to be recorded in multiple exposure photographic films. The velocity information then is extracted from the photographic film by using digital image processing technique.

2.2.3 Directional Ambiguity

One disadvantage of the early PIV technique is that it is not able to determine the direction of the velocity. This is undesirable for the flow field with both forward and reverse flow regions, such as vortex dominated flow in the case of flow over delta wing. Adrian,[44] and Lourenco [45] studied this problem, and proposed the "image shifting technique", or "velocity bias technique" to solve the directional ambiguity of the velocity field. The principle of this technique is to add sufficient artificial shift between consecutive exposures of the particle images. As a result all the velocity vectors are moving in one direction on the photographic film. The true velocity field is recovered by removing the artificial shift in image processing.

In the present investigation, the artificial shift is added by placing a flat mirror in between the flow field and the recording camera. The mirror is oscillating back and forth, and by properly adjust the synchronization, a uniform shift can be added to the flow field.

2.2.4 Optical and Laser Arrangements

The laser used in the experiment is a 18 watt Argon-Ion laser, manufactured by Spectra-Physics (figure 6). The laser has a beam diameter of 1.58 mm and a beam divergence of 0.56 mrad. The operating wave length is a combination of 0.487 μm (blue light) and 0.515 μm (green light). A 24-faceted spinning mirror (Model S225-030-XLIM, made by Lincoln Laser Company) is used here to sweep the continuous laser beam into discrete laser light sheets (Figure 7). It has a diameter of 50.8 mm and a thickness of 9.0 mm. The laser is pointing directly at the spinning mirror, and by rotating at high frequency, the individual face of the mirror sweeps the laser beam into individual laser sheets, and consecutive faces create high frequency discrete laser sheets.

As mentioned before, the PIV photograph records the multiple exposed images of the particles. The number of exposures (n_i) of the particle image strongly affects the quality of the PIV photographic films. Various calibrations have been performed, and it is found out that three to four particle image pairs (n_i =3 or 4) gives the best result:

A mirror (shifting mirror) is used here to provide the velocity shift. The shifting mirror is set at 45° with respect to the centerline of the camera, and it oscillates back and forth around the 45° position. It is properly synchronized with the firing of the camera to minimize the distortion of the flow field. The magnitude of the shift depends on the maximum reversed flow velocity of the flow field investigated. Three factors determine the total shift on the recording film: the magnification of the camera, the peak-to-peak oscillating magnitude of the shifting mirror and the spinning frequency of the spinning mirror. The magnitude of the velocity shift is proportional to camera magnification and peak-to-peak magnitude of oscillation of the spinning mirror, and inversely proportional to the frequency of the spinning mirror. The maximum sweeping angle is normally less than 4.0°.

The setup for PIV investigation of the cross flow is shown in figure 8. Three 12.7 mm flat round mirrors are used to deflect the laser light to the desired position. The coating for the round mirrors is the Argon laser high reflective coating, which provides more than 99% reflection for the 488-514 nm Argon laser lines. The mirror mount, the Newport MM-1 model, allows fine adjustment inside the range of 7.5° of both up / down and left / right. In order to be able to look at the cross flow from the rear, a flat mirror is placed inside the water tank. It is placed at 45° with respect to the trailing edge of the delta wing, and is two root chord lengths away behind the trailing edge. From flow visualization, is it verified that the influence of the mirror on the flow field is trivial. At present setup, in order to cover the area of interest, the mirror has to be at least 6 cm long and 5 cm high. The mirror chosen here is an elliptical flat mirror, with a major axis of 8.08 cm and a minor axis of 5.72 cm, and it is coated with protective aluminum. During the experiments, we found out that the protective coating is not effective to withstand the water corrosion. Currently new coating that is able to resist the water corrosion is being tested. In order to keep the rear view free of distortion, it is necessary that the first surface of this mirror be perpendicular to the base of the water tank, and be placed as close to 45° with respect to the centerline of the delta wing as possible. Care has been taken to make sure the alignments are properly done.

2.2.5 Recording System and Tracer Particle

For dye flow visualization, both camera and camcorder are used to record the flow field. For PIV investigation, only camera is used (figure 9). The camera is a motor driven 35 mm Nikon F-3 SLR camera, with a controllable frequency from 1 frame/second up to 6 frame/second. The lens used is a 200 mm macro lens, which is able to provide close-up look at the area of interest. As Lourenco et al.[46] pointed out, exposure parameters, including exposure time, f- number, and time between exposures, were all important for the quality of the PIV films. In our experiment, these parameters are individually tested. Synchronization of the camera with other components is provided by a Macintosh II computer, using a timing and digital I/O interface (NB-TIO-10 board). The negative film used here is Kodak Tmax-100 ASA film. It is a high resolution film with good sensitivity to the laser light. The camcorder, on the other hand, with its recording frequency of 30 frame/second, is able to provide better temporal resolution of the vortex breakdown process.

The tracer particle used here is silver coated hollow glass bead (Potters Industries Inc.), with an average size of 10 to 15 μm. Initially it mixes well with the water, but because of its density of 1.4 gram / cm^3, it finally tends to sink to the bottom of the water tank.

2.2.6 Image Processing

There are many schemes to extract the original velocity field from the PIV film. Here digital image processing technique is used to recover the original velocity data. The PIV photographic film is scanned by a Nikon Coolscan compact scanner. The scanner has very high resolution (up to 2702 pixel/inch), thus is able to scan the film in great details. The electronically digitized image can then be processed using the standard Fast Fourier Transform Algorithm (FFT). The FFT is incorporated in the software used to process the PIV films. The software allows the selection of a small window around the flow field of interest. Here the window of data processing is chosen to be a rectangular one, with the vertical side half the size of the horizontal side. This is chosen because the velocity gradient in vertical direction is larger, and higher spatial resolution is more desirable there. Currently, The physical size used to process the flow field is 2.0 mm by 1.0 mm. or about 1.5% by 0.8% of the root chord. Because the high power laser light is coming from directly underneath the delta wing surface, there is strong reflection on the surface even though the surface is painted flat black. This is the reason why there are no data available very close to the delta wing surface. One possible solution for this problem is to direct the laser light to the delta wing from side of the water tank. This will avoid the strong reflection from the surface.

The velocity data acquired from the image processing can then be converted into the vorticity data, using the standard central difference scheme.

2.3 Delta Wing Model

The delta wing model is made of Plexiglas. It has a leading edge sweep angle of 60°, and a root chord of 13.0 cm (figure 10). The Reynolds number, based on the root chord and free stream velocity ($U\infty$) of 7.48 cm/s, is 9,800. Both sides of the leading edges are sharp and symmetrically beveled 45° leeward. The delta wing model has a relatively large thickness of 2.54 cm in order to accommodate the reservoir chamber for the trailing edge control jet.

2.3.1 Jet Mechanism

A pair of vectored nozzles are mounted on the trailing edge of the delta wing to provide vectored jet control. The nozzle has a height of 0.51 cm and a span of 4.89 cm, which gives an aspect ratio of 9.6 to 1. The nozzles can be of one of the following configurations: downward symmetric: 45°, 30°, 15°; no angle: 0°; upward symmetric: 15°, 30°; asymmetric: one 30° up and one 30° downward (figure 11). The vectored jet angle is relative to the delta wing surface. A 1/4-Hp aquarium pump that is connected to a 30 gallon reservoir tank is used to provide the trailing edge jet. The jet speed can be varied from 0 to 7.3 $U\infty$. The delta wing is mounted from its bottom surface by two Plexiglas stings (Figure 12). Each of the sting has a 38.1 mm chord, and a cross section of the NACA 0015 airfoil shape in order to minimize the interference it generates with the delta wing flow field. Inside each support, there is a brass tube, which is used to direct the flow from the pump to the two independent settling chambers of the delta wing. The settling chambers are filled with foams in order to ensure a uniform jet output. From visual inspection, it is seen that close to the nozzle, the jet is quite uniform and two dimensional. Further away, axis switching and three dimensionality is observed. Each of the jet supply system

is independent of the other one. With the pump turned on, the flow rate is calibrated and the result is shown in figure 13. No large variation of the flow rate can be observed.

2.3.2 Pitching Mechanism

In order to study the effect of dynamic pitching on the delta wing vortex flow, a drive system is designed. The delta wing is supported at its bottom surface by two stings, which are connected to a pitch/yoke mechanism (figure 14-a). The mechanism is made up of two L-shaped arms and a horizontal center supporting plate (figure 14-b). The mechanism is pivoted about the root quarter chord of the delta wing using a gear/pulley system. The mechanism can pitch the delta wing from 0° to 60° angle of attack. The non-dimensionalized pitch rate, defined as $\alpha^* = (\Delta\alpha / \Delta t\ C)/U\infty$ can be varied from 0 to 0.39. The pitching motion is controlled by a programmable Klinger stepping motor control unit. This unit includes a stepper motor and a CC1.2 motor controller. The accuracy is 0.01° per step. This controller is interfaced with the PS/2 computer through a RS232 interface.

2.4 Dye Flow Visualization Setup

Red food color dye is used as tracer for flow visualization. The delta wing surface is painted white in order to provide the contrast with the dye. The delta wing has black grid line drawn on the surface to indicate the relative position. The root chord is divided into eight uniform sections, and the angle is drawn every 10° from the edge. The red food color dye is held in a small cup attached to the moving platform for the delta wing. At the bottom of the cup there are two individual outlets. One small plastic tube connects each of these outlets to a small (inner diameter 0.05 mm) stainless tube which is glued with silicon at the tip of the delta wing on the lee side. The dye will come out of the tubes through gravitational force, and is entrained into the vortex core. Precaution has been taken to ensure the dye is coming out smoothly and trapped into the vortex core.

3. RESULTS AND DISCUSSION

3.1 Flow Visualization

First, dye flow visualization is carried out to study the dependence of the vortex breakdown on various parameters, including angle of attack, dynamic effect (different pitch rates), and different trailing edge vectored jets. The free stream velocity is set at 7.48 cm/s, corresponds to a Reynolds number of 9,800 based on the root chord. Static angle of attack ranges from 10° to 35° is studied. The non-dimensionalized pitch rate α^* varies from 0.043 to 0.39. However, for the highest pitch rate, the $\alpha^* = 0.39$ case, the free stream velocity is reduced to 5.01 cm/s (Re = 6,700), because the small stepper motor is not able to provide enough torque to pitch the delta wing at this high rate at the Reynolds number of 9,800. There is no noticeable difference of flow behavior within this Reynolds number range. The trailing edge vectored jet velocity can be varied from 0 to 7.3 $U\infty$, and the vectored jet angle can be varied from upward 30° to downward 45° (with respect to the delta wing). Dye is injected through the small tubes near the apex of the wing into the flow to tag the vortex core. Initially, the dye is quite concentrated and straight forward, reflects the motion the vortex core. With the emergence of instability and eventual vortex breakdown, the dye strongly oscillates and quickly disperses away from the vortex core region. Slight back and forth oscillation of the vortex breakdown location is consistently observed at all angles of attacks, which makes it hard to determine the exact location of vortex breakdown. The data presented is the average of the instantaneous vortex breakdown location. Under the normal experimental condition, the uncertainty is estimated to be about ±3% of the root chord.

3.1.1 Static Angle of Attack

When the delta wing is set at a moderate angle of attack, two leading edge vortices form over the delta wing, and the vortex breakdown also appears on the flow field. Here the vortex burst location is measured from the apex of the delta wing. Figure 15 shows the flow visualization results for some of the cases (note: it also include some of the control cases for comparison). At 10° angle of attack, the vortex burst appears at about 76% root chord length from the apex. The burst location then gradually moved to 50% and 25% chord when the angle of attack is increased to 15° and 20°. At 25° angle of attack, the burst locates at 12.5% chord from apex. At 35° angle of attack, total breakdown of the vortex occurs. No organized vortex core can be observed. Further increase of the angle of attack does not show any change of the vortex breakdown pattern. When the angle of attack is less than 20°, the vortex breakdown location changes very fast with the change of angle of attack. Beyond 20°, the vortex breakdown location is less sensitive to the change of angle of attack. The change of the propagation of the vortex burst location can be clearly seen from the breakdown location versus the static angle of attack plot (figure 16, together with the control cases). When the breakdown location x/C is plotted against the angle of attack, two distinct slopes are obvious. The first slope is from 10 to 20°, and the second slope starts at 20°, and ends at 35°. The slow down in the propagation of the vortex breakdown location suggests that at the wing tip portion, the leading edge vortex is more robust, and is less susceptible to the effect of the adverse pressure gradient.

When the trailing edge control jet is turned on, delay of the vortex burst location towards the trailing edge is clearly observed. For example, with the 45° downward vectored jet control, at 10° angle of attack, the vortex breakdown is happening far away downstream of the trailing edge. Even at 15° angle of attack, the breakdown location is still away from the trailing edge (see figure 15). When the angle of attack is increased beyond 20°, the vortex burst location begins to appear on the delta wing surface, and slowly moves towards the apex as the angle of attack increases. Even at 35° angle of attack, where there is total vortex breakdown for the no control case, now there is still about 13% root chord of organized leading edge vortex. This shows that the trailing edge jet control is effective in the whole angle of attack range tested.

To study the effect of different vectored jet angle on the static angle of attack flow field, first it has to be validated that the use of different nozzles themselves will not have noticeable effect on the original flow field. To verify this, flow visualizations of each nozzle configuration at whole angle of attack range and with no control are recorded. As the vortex burst location is concerned, the use of different nozzle configurations shows very little difference from the 0° nozzle configuration. This justifies that the effect of trailing edge jet control solely comes from the vectored jet, and not from the use of different nozzles themselves.

3.1.1a Symmetric Control

The effect of the vectored jet angle on the vortex breakdown is studied using five symmetric nozzle configurations: 15° upward, 0°, and 15°, 30°, 45° downward. The jet velocity is set at maximum to show the maximum effect. The 0° no control case is included for comparison. For the upward 15° vectored jet case (see figure 16), at low angle of attack, it shows small delay of the vortex burst location. When the angle of attack is higher, this favorable effect diminishes. The 0° jet control case show a consistent improvement over the no control one. For all the angles of attack, except the 35° case, it shows a near consistent improvement of about 10% chord length. At 35°, this value decreases to about 5%. When the vectored jet is directed downward, significant improvement shows up. For example, for the 30° downward vectored jet case, the maximum delay is more than 40% chord length, and even at 35° there is still about 13% chord of leading edge vortex stays unbursted. From figure 16, we can clearly see these trends: (1) all of the vectored jet cases show improvement in delaying the vortex burst; (2) upward trailing edge vectored jet is less effective than the 0° jet; (3) downward vectored jet is much more effective than 0° control jet, and the higher the downward jet angle, the more effective the control will be; (4) when the angle of attack of the wing is less than 20°, the net delay of the vortex burst location increases with the increase of angle of attack, when the angle of attack exceeds 20°, the net delay will decrease.

The breakdown of the leading edge vortex is caused by the adverse pressure gradient that exists along the vortex axis. The trailing edge jet will create a local stream-wise favorable pressure gradient at the trailing edge, thus effectively alleviate the overall adverse pressure gradient imposed by the outside flow. The trailing edge jet will also entrain the flow along the vortex axis and increase the transportation of vorticity along the vortex core, which is essential to relief the accumulation of upstream vorticity. These will effectively delay the vortex breakdown process. Compare the upward and downward vectored jet of the same angle, the upward jet has a velocity component normal to the delta wing surface that serves to "push" the vortex core up and away from the delta wing surface, thus tends to make the vortex more unstable. The favorable

effect provided by its velocity component along the wing surface is offset by this adverse effect. That is why its effectiveness is limited. The downward vectored jet, on the other hand, has a downward velocity component perpendicular to the wing that will "pull" the vortex core down to the delta wing surface, which stabilizes and strengthens the vortex. This combined with the favorable effect created by the velocity component along the delta wing surface, create a much more significant effect. From the experiment, it is seen that the vectored jet angle plays a very important role in delaying the vortex breakdown.

3.1.1b Asymmetric Control

In order to study the effect of asymmetric trailing edge jet control, a nozzle configuration with one upward 30° and one downward 30° nozzle is tested. The left side vectored jet is directed downward and the right side jet is directed upward (Figure 17). A typical flow visualization result of the asymmetric control case is presented in figure 18. This flow visualization corresponds to 25° angle of attack of the delta wing and the vectored jet velocity is set at maximum. At the left side, the favorable pressure gradient produced by the downward vectored jet significantly delays the vortex burst location while the right side jet shows very little favorable effect. It is important to note that this asymmetric vortex breakdown pattern is consistently observed throughout the asymmetric vectored jet control experiments. This suggests that the asymmetric effect produced by the asymmetric trailing edge vectored jet control is robust. It also shows the potential to use this effect to control the adverse effects that are caused by the asymmetric vortex breakdown over the delta wing. To compare the effect of symmetric control and asymmetric control, four cases are presented on the vortex burst location versus the angle of attack plot (figure 19). The four cases are: 0° nozzle, no jet control; 30° asymmetric upward vectored jet; 30° asymmetric downward vectored jet, and 30° symmetric downward vectored jet. From the plot, we can see that the upward asymmetric jet shows some favorable effect at low angle of attack, but when the angle of attack is over 25°, the favorable effect virtually disappears. The asymmetric downward jet control shows consistently large improvement over the no control case. Especially at high angle of attack, this favorable effect is more pronounced. For example, at 35° angle of attack, it still shows a 17% chord of organized vortex core. Especially at high angle of attack, the asymmetric vortex breakdown pattern caused by the asymmetric trailing edge jet control is prominent. Compare the effect of the asymmetric downward jet with that of the symmetric downward one, we can see that for most of the angle of attack cases tested, the symmetric vectored jet control shows more favorable effect than the asymmetric one. An interesting phenomenon to note is that the 30° upward asymmetric jet is actually more effective than the 15° upward symmetric jet. These are probably due to the interaction between the upward vectored jet and downward vectored jet. The interaction will try to average the effects of the two different jets. As a result, the downward asymmetric control jet will be less effective than the corresponding symmetric control case. On the other hand, the upward asymmetric jet will be more effective than the corresponding symmetric control case.

3.1.1c Vectored Jet Velocity

Trailing edge control jet velocity also has large effect on the vortex breakdown. A 0° nozzle configuration at 20° angle of attack and a 45° downward nozzle configuration at 20° angle of attack are chosen to study the effect of jet velocity on vortex breakdown. The jet velocity U_j

can be varied from 0 to 7.3 times of the free stream velocity U∞. Different jet velocity is achieved by adjusting the valve on the jet system, and the jet is calibrated before each experimental run. This adjustment is accurate and the position adjustment is repeatable (within 2%). The effect of jet velocity on vortex breakdown are plotted in figure 20 in the form of vortex breakdown location versus the jet velocity for the two cases (the data from Helin et al.[47] are also included for comparison).

For the 0° vectored jet control case, when the velocity of the jet is set at 1.0 U∞, no delay of the vortex breakdown location is observed, further increase the jet velocity to as high as 5.0 U∞, the delay of the vortex burst location is still less than 2% chord. When the jet velocity is further increased, noticeable improvement begins to show up. At 6.0 U∞, the delay of the vortex burst location increases to about 5%. With maximum jet velocity, the improvement is about 9%. In general, the effectiveness of the 0° vectored jet is not large.

The more significant change happens in the 45° downward vectored jet control case. Even at very low velocity (U_j = 1.0 U∞), the favorable effect already shows. When the vectored jet velocity increases to 2.0 U∞, the vortex burst location is pushed back towards the trailing edge in a similar pace as the 1.0 U∞ case. When the vectored jet velocity further increases, drastic improvement shows up. At a velocity of 2.6 U∞, the jet delays the vortex burst location for more than 18% root chord, and this favorable effect continuous to grow, in a slightly slower pace, until it reaches its maximum improvement when the jet is at maximum velocity, which is a net 58% root chord delay, or, in other words, a 270% improvement over the no control case.

The difference of these two vectored jet configuration is the angle of the vectored jet. Because the downward vectored jet shows a much more favorable effect than the 0° jet, here once more, we speculate that the jet velocity component normal to the delta wing surface plays a more important role in delaying the vortex breakdown.

From figure 20, it is seen that both of the two cases show a threshold on the vortex breakdown curves, although the 45° downward control case is more significant. The threshold is defined as the large change in the slopes of the curves. The trailing edge control jet will create a local stream-wise favorable pressure gradient region near the trailing edge, and this favorable pressure gradient region will relieve the overall adverse pressure gradient imposed by the external flow and also strengthen the leading edge vortex flow. We may expect the favorable pressure gradient created by the trailing edge jet to be proportional to its strength, or the jet velocity. When the jet velocity is low, its favorable influence is limited to a small local region, and the effect of the jet is very limited. Until the jet velocity is sufficiently high so that its influence can be 'felt' upstream, then the increase of the jet velocity will result in a more drastic delay of the vortex burst location. This will explain the existence of the threshold. From the plot we can see that the threshold for the 45° vectored jet (2.0 U∞) is much smaller than the 0° control jet case(5.0 U∞). That also shows the downward control to be more effective, as it only needs a weaker control jet to achieve the same effect. Considering that the larger the downward vectored jet angle, the more effective the control is, thus the threshold for the other downward control jet cases may appear at a jet velocity between 2.0 U∞ to 5.0 U∞.

Helin et al. also studied the effect of trailing edge jet velocity using a 8:1 aspect ratio rectangular 0° trailing edge jet, based on a 60° delta wing model. Their result is also presented in figure 20 for comparison. Their data showed a consistently larger (favorable) x/C value for the vortex breakdown location as compared to our 0° jet case. Because their delta wing model

has a much smaller thickness (6.35 mm, as compared to 25.4 mm of our model), we may deduce that decrease the thickness of the delta wing will have favorable effect on leading edge vortex breakdown.

Another way to study the effect of trailing edge control jet on the leading edge vortex flow is to study the change of vortex core angle. The vortex core angle is defined as the angle between the centerline of the delta wing and the vortex core (marked by the dye). For all the no control static cases in which the dye is not totally breaking down, the vortex core strictly assumes a 19°±1° direction. When the trailing edge control jet is turned on, only very slight decrease of the vortex core angle (1°-2°) can be observed down stream close to the trailing edge. Close to leading edge, no noticeable change can be observed. This suggests that the leading edge separation of the flow is a relatively robust process, and is not easily subjected to the influence of the trailing edge jet. Although the trailing edge jet has significant effect on enhancing the leading edge vortex flow, the vortex core relatively stays unchanged.

Once more, the results are compared with that of Helin et al.. Their data showed a 17°±1° angle for the vortex core, and they also suggested that the trailing edge jet did not have any noticeable effect in changing the direction of the vortex core. Since under the same conditions, their vortex breakdown location is more closer to the trailing edge than what we have, and their vortex core angle is smaller, so we may assume that smaller vortex core will corresponds to a more stable leading edge vortical structure.

For all the experiments, the delta wing is exclusively impulsive-started. The leading edge vortex needs time to establish. To study the effect of impulsive start on the flow structure, flow visualization using a 0° symmetric nozzle with no trailing edge control jet are documented and plotted here in figure 21. It is seen here that for different angle of attack, the leading edge vortex takes different time to establish. Here we define the steady state as the state that the leading edge vortex breakdown location stays unchanged. At 10° angle of attack, it takes about 12 seconds for the vortex to reach its steady state. At 20° angle of attack, this value decreases to about 8 seconds. At 30° angle of attack, it further decreases to about 6 seconds. In general, the leading edge vortex takes less time to establish when the angle of attack is higher. Impulsive-start at a certain angle of attack is essentially pitching from 0° to that angle of attack using infinite pitch rate, at high angle of attack, the adverse pressure is more severe, so whenever the leading edge vortex breakdown sets in, it will be pushed to its steady state much faster. Because 10° is the minimum angle of attack used in the experiments, all data for the experiments are taken later than 12 seconds after the impulsive-start of the delta wing to ensure no initial unsteady effect is involved.

3.1.2 Dynamic Pitching

When the delta wing undergoes ramp-type pitching up motion, the delay of the onset of the vortex breakdown to a higher angle of attack as compared with static case is consistently observed. This delay of the vortex breakdown is closely associated with the dynamic effect of the pitching motion. Here experimental investigation of a non-dimensionalized pitch rate ranges from 0.043 to 0.39 are carried out to study the dynamic effect. The pitching motion is a ramp-type, single pitch-up motion from 10° to 45° angle of attack. The vortex breakdown location is measured from the apex of the delta wing, and is plotted against the wing's instantaneous angle

of attack (or pitching time) for all these pitch rates. The static angle of attack with no control jet case is also included for comparison.

3.1.2a Pitching Without Control Jet

Figure 22 shows the result of the pitching motion with no trailing edge control jet. When the delta wing undergoes the ramp-type pitching motion, the vortex burst location consistently shows a very large initial delay, even at very low pitch rate, and this initial delay appears to be insensitive to the variation of the pitch rate. For example, at the lowest pitch rate of $\alpha^* = 0.043$, when the delta wing starts to pitch up at 10° angle of attack, the vortex bursts at about 85-90% root chord from the apex, which is an improvement of 10-15% root chord over the static case. As the pitching motion continues, this favorable effect, which is due to the unsteady effect, also continues. At the low pitch rate of $\alpha^* = 0.043$ case, the leading edge vortices appear to behave quasi-steadily after they experience the initial unsteady effect. This is marked by the two distinct slopes on the breakdown location versus angle of attack plot, which is similar to the two distinct slopes for the static case. When the pitch rate is increased, the unsteady effect becomes more dominant, and the leading edge vortex behaves quite differently from the quasi-steady state. For higher pitch rates, the vortex can stay unbursted much longer for the same angle of attack. For example, for the highest pitch rate, $\alpha^* = 0.039$, the vortex can stay unbursted for about 45% chord length even at 35° angle of attack. At this angle of attack, there is already total breakdown of the vortical structure for the static case. It is interesting to note that for all the pitch rates, at high angle of attack, the breakdown location seem to be varying linearly with the increase of the angle of attack, which means at higher angle of attack, the propagation speed of the vortex breakdown location reaches a stable speed. The effect of pitching on the vortex breakdown can be explained as follows: when the delta wing undergoes pitching-up motion, the leading edge vortex flow takes time to establish under the new angle of attack. When it finally responds to the change in the angle of attack, the delta wing already pitches to a higher angle of attack. That is why compare the vortex breakdown for the same angle of attack cases, the dynamic pitching case shows the vortex breakdown location to be more closer to the trailing edge.

3.1.2b Pitching With Control Jet

From the static angle of attack experiments, it is already demonstrated that trailing edge vectored jet has significant favorable effect on the leading edge vortex flow. Here a 45° downward symmetric vectored jet configuration with maximum jet velocity is chosen to study the coupled effect of vectored jet and dynamic pitching (figure 23).

The independence of the initial delay from the pitch rate is seen to be more prominent. For all the pitching cases, no vortex breakdown has been observed over the delta wing surface at angle of attack less than 15°. Initially, all of the curves are overlapping on one another, when the pitching motion continues, the curves separate. This suggests that, at the initial stage, the flow is dominated by the effect of jet, when the pitching motion continues, the dynamic effect of pitching gradually sets in, and later becomes dominant. Here even for the smallest pitch rate, $\alpha^* = 0.043$ case, the leading edge vortex flow already shows large departure from the quasi-steady behavior. In general, the pitching with vectored jet cases show vast improvement over the previous pitching only cases. Here even the lowest pitch rate of $\alpha^* = 0.043$ with jet control is

overall more effective than the $\alpha^* = 0.26$ with no jet control case. This shows the combined favorable effect induced by the trailing edge vectored jet and the dynamic pitching.

In order to study the propagation speed of the vortex breakdown location, here the vortex burst location is plotted against the non-dimensionalized pitch time ($t^* = tU\infty/C$), instead of angle of attack, for both the no control(figure 24) and with control (figure 25) cases. From these two plots, we can see that the higher the pitch rate, the faster the vortex burst point moves upstream to the apex.

To show the unsteady effect and its coupled effect with vectored jet, the slope of the vortex burst location versus the angle of attack, i.e., $\Delta x/(C\Delta\alpha)$, for both control and no control pitching cases, are calculated using least square fit (from figure 22 and 23). The results are plotted against the pitch rate in figure 26. The value $\Delta x/(C\Delta\alpha)$ measures the movement of the vortex burst location with respect to the change of the angle of attack. A lower value here means that with the same amount of change in the angle of attack, the vortex breakdown location only moves a shorter distance, i.e., the leading edge vortex is less susceptible to the pitching effect, and thus more stable. For both the control and no control cases, the pitching motion shows a stabilizing effect for the leading edge vortex as it is clear that the value $\Delta x/(C\Delta\alpha)$ is decreasing with the increase of the pitch rate. In other words, the upstream propagation of the vortex breakdown location with respect to the change of the angle of attack actually slows down when the pitch rate is increased. Here the favorable effect of jet is demonstrated by the consistently lower value of $\Delta x/(C\Delta\alpha)$ for the control case as compared to the no control one. Compare the two curves, it is easy to see that the curve corresponds to jet control case is similar to the curve for no control case, but with much smaller value. This means that for all these pitch rates, the vectored control jet is very effective in slowing down the propagation of the vortex breakdown location. Another interesting pattern for both of the two cases is that, when the pitch rate increases from the lowest value, first the value $\Delta x/(C\Delta\alpha)$ will decrease quickly, when the pitch rate is high ($\alpha^* = 0.26$), further increase of the pitch rate results in a much slower decrease of the value $\Delta x/(C\Delta\alpha)$. At low pitch rate, the unsteady effect is small, the leading edge vortex flow still assumes some quasi-steady behavior. When the pitch rate increases, the unsteady effect becomes dominant, and its effect in delaying the vortex breakdown is also getting stronger, so the value of $\Delta x/(C\Delta\alpha)$ is pushed down quickly. When the pitch rate is high enough, as for the $\alpha^* = 0.26$ case, the unsteady effect is already established and dominant, so further increase of the pitch rate will result in less improvement.

There is another way to study the unsteady effect, that is, by looking at the dependence of vortex burst location on the non-dimensionalized time $t^* = tU\infty/C$. Here the slope of the vortex burst location versus the t^* is acquired using least square fit (from figure 24 and 25), and the slope is plotted against the pitch rate. Both the with and without control cases are plotted in figure 27. For the no control case, at the lowest pitch rate of $\alpha^* = 0.043$ case, the propagation velocity of the breakdown point U_p is about 10% of the free stream velocity. When the pitch rate increases, the propagation speed also increases. At $\alpha^* = 0.39$, U_p is about 47% of the free stream velocity. This suggests that the unsteady effects actually accelerates the vortex breakdown process. This seems to be contradicting with the fact that the propagation of vortex breakdown location is actually delayed by increasing the pitch rate, as we just discussed. This paradox can be explained as follows: Initially, the vortex structure can not quickly respond to the fast pitching motion, thus the vortex breakdown location stays the same even when the delta

wing is already pitched to higher angle. However, whenever the vortex breakdown is initiated, the leading edge vortex is going to experience a much more severe adverse pressure gradient as compared with the static case. The adverse pressure gradient imposed by the external flow will become more severe. Under this adverse pressure gradient, the vortex breakdown process is going to accelerate. The higher the pitch rate, the more severe the adverse pressure gradient, thus the faster the breakdown point will be propagating. On the other hand, the delta wing will take much less time to reach high angle of attack in the high pitch rate case. So the final effect lies in the competition between the two factors. Actually, the factor $U_p/U\infty$ can be written as:

$$U_p/U\infty = (\Delta x/\Delta t) / U\infty = [\Delta x/(C\Delta\alpha)] / [(C\Delta\alpha/\Delta t)/U\infty]$$
$$= [\Delta x/(C\Delta\alpha)]\ \alpha^*$$

So the factor $U_p/U\infty$ is actually linked to the factor $\Delta x/(C\Delta\alpha)$ by the non-dimensionalized pitch rate α^*. Here the propagation speed $U_p/U\infty$ varies from 10% at the lowest pitch rate to about 47% at the highest pitch rate, with a factor for about 5, while the pitch rate α^* varies from 0.043 to 0.39 for a factor of 9. Therefore the pitching motion can more than compensate the adverse effect of the upstream acceleration of the vortex burst point, and still provides overall favorable effects for the leading edge vortex.

3.2 PIV Measurements

In order to study the behavior of the leading edge vortex flow quantitatively, PIV measurements are taken along selected planes. The PIV technique is in general a two dimensional technique that is able to provide accurate instantaneous whole field velocity information. . Here two sets of planes are selected to study. The first set is stream-wise plane. The second set includes several cross-flow planes. The plane parallel to the free stream is defined as the stream-wise plane, and the plane normal to the free stream is defined as the cross-flow plane. The planes are so selected in order to show the leading edge vortex flow structure from different points of view.

3.2.1 Stream-wise Plane

Here a plane that is parallel to the free stream is selected. The plane is located 36% root chord away from one corner of the delta wing. The sectional chord length of the selected plane is 62.5% of the root chord (figure 28).

First the angle of attack of the delta wing is set at 10°. PIV results have been acquired for three cases: no control, 15° downward and 45° downward vectored jet control. Three instantaneous velocity fields, one corresponds to each case are shown in figure 29. For the no control case, at the left side, the velocity profile is discontinuous and shows a very large upward motion. This suggests that at that region, the local leading edge shear layer is wrapping up and penetrating this plane, which causes the local flow to go up. Downstream of this location, large deficiency of the velocity profile occurs, the location corresponds to about 77% of root chord from the apex, which indicates the emergence of vortex breakdown. This is consistent with the dye flow visualization result, which shows the vortex burst location for the 10° static case to be at about 76% chord. Close to the delta wing surface and near the trailing edge, the velocity

vectors show the tendency to move up and away from the surface. The local trailing edge flow stream is estimated to have a magnitude of 1.1 U∞, and assumes a downward angle (with respect to the free stream) of 25.2°.

As the 15° downward vectored jet is turned on, the discontinuity of velocity that appears on the no control case is replaced by an overshoot of the velocity. At the left, the magnitude of the upward velocity component is also reduced. At the region where large velocity deficiency appears for the no control case, the velocity deficit is still visible, but largely reduced. Another distinct effect is the enhancement of the downward flow near the trailing edge. Not only is the magnitude of this downward flow increases, but it also assumes a larger downward angle with respect to the surface. Here the local trailing edge flow is estimated to have a velocity of 1.5 U∞, and a downward angle of 39.9°. When the vectored jet angle is set at 45°, more favorable effects are observed. Here the velocity strongly overshoots at the left, and the upward flow tendency is replaced by a downward one, indicating the flow is moving closer to the wall. The original velocity deficit region is replaced by velocity overshoot region, indicating very large entrainment of flow along the vortex axis that strongly accelerates the axial velocity at the vortex core. Over the whole field, the velocity is accelerating rapidly and turning sharply down right behind the trailing edge. The magnitude of the velocity close to the trailing edge is measured to be 1.9 U∞, and the downward flow angle is increased to 46.7°.

From the previous discussion, we can see that entrainment effect of the vectored control jet accelerates the axial flow over the delta wing, and thus essentially increases the axial velocity of the vortex core. This will increase the transportation of vorticity along the vortex core, thus relief the accumulation of vorticity on the upstream vortex core region. In addition, the axial velocity acceleration induced by the trailing edge jet will alleviate the overall adverse pressure gradient along the vortex core, and further enhance the vortex flow.

When the angle of attack is increased to 20°, large scale vortex breakdown is clearly observed for the no control case (figure 30). The velocity field closely resembles the wake behind a bluff body, which is characterized by large velocity deficits and even regions of flow reversals. Close to the sectional leading edge region, the velocity vectors near the surface show large upward component, and there is strong flow along the wing surface at the rear. This suggests that the vortex breakdown has already happened upstream of the sectional leading edge, and is lifted away from the wing surface. The flow reversal occurs about 40% sectional chord from the sectional leading edge, and resumes the forward flow downstream at the sectional trailing edge.

When the 15° downward control jet is turned on, improvement of the flow field is observed. The wake-type region still exists, but it moves downstream and the size is much smaller. On the other hand, this region is closer to the wing surface, indicating the breakdown is occurring closer to the wing surface. The velocity deficit recovers more quickly now. Close to the trailing edge, there is a similar accelerated downward flow pattern as in the corresponding 10° angle of attack case. When the 45° downward control jet is turned on, no noticeable breakdown phenomenon can be observed for the whole flow field. At the left side of the plane, very strong upward overshoot of the velocity occurs, followed by sharp downward turning of the flow towards the surface. This suggests that the leading edge shear layer is first rolling up, penetrating this plane, and then rolling down, leaving the plane. Large acceleration of the flow along the surface is also observed and the velocity assumes a more parallel direction to the wing

surface. Both the two control jet cases show the tendency that the entrainment of the flow by the trailing edge control jet tends to pull the leading edge vortex down close to the surface. This will stabilize the leading edge vortex and reduces the relative angle of the vortex core with respect to the delta wing surface. This essentially is equivalent to the decrease of the "effective" angle of attack of the delta wing. The result is the alleviation the adverse pressure gradient posed by the external flow, and the effective delay of the vortex breakdown process.

3.2.2 Cross-flow Measurement

For all the data presented here, the delta wing is set at 12.5° angle of attack. The cross flow plane is chosen to be normal to the free stream. Five cross flow planes are selected here, they correspond to 50%, 58%, 67%, 72% and 92% root chord length away from the apex of the delta wing. The flow visualization result indicates that the vortex breakdown occurs at about 67% root chord from apex for this static case. To study the effect of the vectored jet on the vortex breakdown process, downward 45° vectored jet with $U_j = 3.0\ U\infty$ and $U_j = 7.3\ U\infty$ are studied on the 92% cross section case.

3.2.2a Before Vortex Breakdown: 50% and 58% Chord

From dye flow visualization, it is determined that at 50% chord there is no vortex breakdown for the no control case. Figure 31 shows one instantaneous velocity field and the associated vorticity field. It can be seen that the flow separates from the left sectional leading edge and forms a free shear layer. The shear layer is subject to Kelvin-Helmhoz type instability and quickly rolls into discrete vortices. Here one of the vortical structures is engulfed into the primary vortex. The instantaneous vorticity field shows a quite different pattern as compared with those obtained from other experimental investigations using conventional single-probe measurement technique. It is because many of the distinct features of the leading edge vortex are time-dependent, and they are averaged out by the use of traditional single-point measurement techniques. In order to study the basic flow structures of the instantaneous flow fields, twenty five consecutive instantaneous velocity and the corresponding vorticity fields are processed. The instantaneous pictures are taken at four frames per second. Complete sequences of the unsteady variation of the vortical structures are observed.

A global picture of the variation of the flow structures can be seen from the plot for the instantaneous circulation of the primary vortex (figure 32). Here the circulation is calculated using a fixed rectangular box that encloses the primary vortex of the averaged vorticity field. The box is from 7.5% to 22% root chord horizontally, and 1.2% to 12.5% root chord in the vertical direction, measured from the delta wing tip of the local cross section. The plot clearly shows quasi-periodic variation of the circulation of the primary vortex. Note on the plot (a), (b), and (c) correspond to the three distinct flow structures we will discussed below. The match between the variation of circulation and the different vortical structures clearly justifies the quasi-periodic behavior of the primary vortical structure.

Figure 33 shows a sequence of three distinct instantaneous vortical structures. In figure 33(a), the primary vortex is coherent with well organized structure. The vortex core is clearly defined and the size of the primary vortex is large. Under the influence of Kelvin-Helmhotz Type instability, part of the shear layer rolls into discrete vortical structures, and one of them is engulfed by the primary vortex. Most part of the free shear layer still stays at the left bottom

corner. The strong leftward flow of the primary vortex close to the delta wing surface induces large leftward boundary layer flow. The boundary layer separates as a result of the cross-sectional adverse pressure gradient, and rolls into a secondary vortex. The secondary vortex (plotted in dotted lines) rotates in opposite sense as the primary vortex. The interaction between the primary vortex and the secondary vortex will lift both vortical structures up and away from the surface. On the vorticity plot, it is clear that as a result of this interaction the primary vortex is lifted up, and the secondary vortex is also being ejected upward. The movement of the secondary vortex essentially cut off the link between the free shear layer and the primary vortex.

The strength of the primary vortex depends on the continuous feeding of the vorticity from the upstream free shear layer. The cut off of their linkage quickly weakens the strength of the primary vortex, as seen here on figure 33(b). The size of the primary vortex now is greatly reduced, and the vortical structure is less coherent. The primary-vortex-induced secondary vortex is also weakened, and their interaction is not strong enough to lift the primary vortex up. As a result the primary vortex falls down close to the surface. These result in the fact that some of the areas that used to be occupied by the primary vortex now is free of vorticity. The shear layer will respond to this by quickly filling in these areas. The results are, first, the local leading edge free shear layer is going up and grow in strength in an attempt to connect to the primary vortex, with a side effect to suppress the secondary vortex, to keep it from moving upward; secondly, the upstream shear layer is moving to a position right on top of the primary vortex, and connects to it. The upstream shear layer not only serves to feed the primary vortex, which greatly increases its strength, it also press down on the primary vortex to make the vortical structure more compact in size. The secondary vortex here is growing leftward horizontally, underneath the local free shear layer.

As seen here on figure 33(c), the primary vortex is more concentrated than before. Now the primary vortex core is going up. Part of the free shear layer is engulfed into the primary vortex, and the remaining part is coming down to the surface. With the strengthen of the primary vortex, the secondary vortex is also growing in strength. With the process of their interaction continues, the primary vortex will be pushed up, breaking away from the free shear layer, and rolls into discrete and more coherent vortical structure. This mark the end of this cycle, and the beginning of a new one.

The averaged velocity and vorticity fields are shown in figure 34. Clearly the averaged plot show a much more coherent structure than the instantaneous case. It is easy to see that most of the distinct features of the instantaneous vorticity plot already disappear, thus much less information can be acquired from the averaged data. This suggests that in order to clearly understand the fundamental behavior of the leading edge vortex flow, instantaneous and whole-field measurement technique, such as PIV, is necessary. The peak vorticity level for the averaged vorticity field is less than half of the instantaneous peak value because of the time-averaging process. On the other hand, the integrated quantity, such as the total circulation, shows only small difference.

The overall structure for the 58% chord case shows very little difference as compared with the 50% case. The primary vortex is slightly expended, and the peak value is less. It should be noted that the quasi-periodic variation of the instantaneous vortical structures as we discussed above is also observed at this cross section.

3.2.2b Vortex Breakdown: 67%, 75%, and 92% Chord

From flow visualization it is determined that the vortex undergoes breakdown process at 67% chord. Figure 35 shows one of the instantaneous velocity and the corresponding vorticity field at this cross-section. Here the primary vortex already loses its concentration, and breaks into several discrete vortical structures, with no distinguishable vortex core. Patches of negative (counterclockwise) vortical structures have penetrated into the center region of the vortex. The peak value of the instantaneous vorticity is about half that of the corresponding 50% case. At 75% chord, the instantaneous flow field shows random flow pattern all over the plane. No large scale coherent vortical structure can be found. At 92% chord, the flow field displays a total random pattern. Instantaneous vorticity field shows very weak vortical structure.

The averaged vorticity fields (figure 36) shows less information as compared with the instantaneous ones. The averaged field corresponds to the 67% case still show a well organized structure, but with no distinguishable vortex core, the peak magnitude of vorticity decreases drastically. The strength of the primary vortex decreases, and the primary vortical structure expands. 75% chord case sees a further decrease in the peak vorticity magnitude, and expansion of the primary vortex, but the primary structure is still clear. No distinct vortex core can be seen. At 92% the vorticity plot shows an overall low vorticity level, with near-zero vorticity region surrounds the estimated vortex core. The averaged cross flow velocity in the vortex core region is also very low.

Circulation of the averaged primary vortex for the five different cross sections are calculated and plotted in figure 37. Before vortex breakdown, because of the entrainment effect of the primary vortex, its circulation grows quickly, in a nearly linear growth rate, until it reaches the maximum value at the breakdown location. Once the vortex breakdown is initiated, the suction peak of the primary vortex quickly disappears. As a result the circulation quickly decreases. Further down stream, the flow partially recovers from the vortex breakdown, but the circulation level is less than the peak value reached right before vortex breakdown .

From the averaged file, the averaged vorticity value of the estimated vortex core for each cross section is calculated. Figure 38 shows the vorticity variation. The peak vorticity quickly dropped from 92.6 at the 50% chord, to 65.1 at 58% chord, and further down to 25.0 at 68% chord at an almost constant rate, which signifies that the vortex core has already been losing its suction peak because the vortex flow is experiencing a very large adverse pressure gradient. Once the vortex breakdown starts, this drop slows down, as the flow no longer faces the strong adverse pressure gradient. The vorticity level for the estimated vortex core region approaches zero further down stream.

3.2.2c With Trailing Edge Jet Control: 92% Chord

The effect of trailing edge control jet is studied using 45° downward vectored jet at the 92% chord cross section. Two jet velocities are tested: $U_j = 3.0\ U\infty$ and $U_j = 7.3\ U\infty$.

When the vectored jet velocity is set at 3.0 U∞ (figure 39), the primary vortex becomes visible, the free shear layer is strong, and the primary vortex begins to show a coherent structure with clearly defined vortex core. The vorticity level at the vortex core is about 35.0, a value larger than the no control 60% chord case. This signifies the recovery of the suction peak of the vortex core. At this angle of attack, this vectored jet strength is just enough to push the breakdown location away from the delta wing surface.

When the jet is set at maximum velocity, the effects becomes more pronounced (figure 40). The primary vortex shows a very coherent structure, with the vorticity level at the vortex core reaches 78.0, which represents a strong suction peak. The total circulation for the primary vortex increases about 20% as compared with the no control case. It is also quite clear that, with the jet control, the primary vortex is also much more compact in size.

As the PIV experiments along the streamwise direction already show, the trailing edge vectored control jet induces strong accelerated flow along the vortex core. The local favorable pressure gradient induced by the vectored jet will alleviate the adverse pressure gradient imposed by the external flow. With the enhancement of the axial velocity, the transportation of vorticity along the vortex axis also increases. On the cross flow plane it is seen that the vectored jet strongly enhances the primary vortex, as both the suction peak and the circulation of the primary vortex are much stronger. The overall effect is that the leading edge flow is much more robust and stable with the trailing edge jet control.

3.2.2d Swirl Velocity

The swirl velocity inside a leading edge vortex system plays an important role in determining the stability of the vortex flow. For example, it had been shown [13] that, under a quasi-cylindrical vortex assumption, the high the swirl velocity, the more severe the adverse pressure gradient will be, as compared with the pressure gradient outside the vortex core. In other words, The flow with higher swirl velocity will be more unstable, if the other conditions remain the same. Although the delta wing flow field is not axisymmetric, the quasi-cylindrical assumption is still expected to be valid, at least qualitatively. Here the swirl velocity measured at a profile normal to the horizontal plane and through the vortex core is presented in figure 41. The profiles are from the averaged velocity files, and the data correspond to 50%, 58%, 67% and 75% chord are chosen. Since at 92%, no distinguishable vortex core can be found, only one corresponding control case is presented. It is apparent from the plot that the flow is far from axisymmetric. The swirl velocity close to the wing surface (leftward flow) has a much higher magnitude. For example, for the 50% chord case, the maximum swirl velocity is more than 1.5 $U\infty$ for the leftward flow, whereas the maximum swirl velocity above the vortex core (rightward flow) is less than half of that value. For the cases corresponding to no breakdown regions, the 50% case and the 58% case show very similar pattern. Starts from the 67% chord case, where the vortex breakdown is initiated, the swirl velocity becomes markedly different, especially at the region underneath the vortex core. The magnitude of the swirl velocity under the vortex core drops much more quickly compared with the before breakdown cases. The maximum leftward velocity decreases to less than 1.2 $U\infty$ for these cases, and the profile is flattened out at the tip. The subcore size, defined as the vertical distance between the points with maximum leftward and rightward swirl velocities, becomes markedly expanded.

When the control jet is used, very large effects can be observed. The swirl velocity shows a very similar pattern as the 50% no control case (actually, the two curves almost overlaps), which means that the subcore size is marked reduced compare with no control case, and the swirl velocity is markedly stronger. Here no flatten out of the velocity profile can be seen. Instead of becoming more unstable as predicted by the previous pressure gradient argument, the leading edge vortex becomes more stable. The reason is, although the swirl velocity greatly increases, so does the axial velocity. As a result the swirl angle does not change

very much. Increasing the swirl velocity essentially strengthens the primary vortex, and increasing the axial velocity effectively relief the accumulation of upstream vorticity on the vortex core region, and alleviates the adverse pressure gradient along the vortex core. So the overall result is that the favorable effect induced by the trailing edge vectored jet is dominant over the unstable effect.

4. CONCLUSIONS

The thrust-induced effect on a pitching-up delta wing flow field is studied experimentally in a water towing tank facility. Both dye flow visualization and Particle Image Velocimetry (PIV) techniques are used.

From dye flow visualization, it is shown that upward trailing edge jet control shows very little favorable effect in delaying the vortex breakdown. For both static and dynamic pitching cases, the downward trailing edge vectored jet is always very effective in delaying the vortex breakdown. The higher the downward vectored jet angle, the more effective the control is. The trailing edge vectored jet velocity also has large effect in delaying the vortex breakdown, increasing the jet velocity results in further delay of the vortex breakdown. From the PIV measurement along the stream-wise plane, it is found that the trailing edge jet entrains strong flow along the vortex axis, thus effectively accelerates the axial velocity on the vortex core region. On the cross-flow plane, the existence of trailing edge control jet significantly enhances the primary vortical structure. The entrainment effect of the trailing edge control jet along the vortex core increases the transportation of vorticity along the vortex axis, and essentially relieves the accumulation of vorticity on the upstream vortex core. On the other hand, near the trailing edge, the vectored jet induces a local favorable pressure gradient along the vortex axis, thus effectively alleviate the overall adverse pressure gradient that causes the vortex breakdown.

An asymmetric trailing edge nozzle configuration is tested to show the effect of controlling asymmetric vortex breakdown. It is shown that the asymmetric (one nozzle pointing 30° upward, one 30° downward) trailing edge jet induces a consistently asymmetric vortex breakdown pattern, this pattern is more prominent at high angle of attack. This shows the potential to utilize the asymmetric trailing edge jet to control the asymmetric vortex breakdown pattern.

The dynamic effect of ramp-type pitching-up motion on the vortex breakdown process is also studied. The delta wing is pitched from 10° to 45°, and the non-dimensionalized pitch rate varies from 0.043 to 0.39. From dye flow visualization, it is found out that there is always a large initial delay associated with the starting of the pitching motion. The initial delay is insensitive to the pitch rate. At low pitch rate, the flow still behaves quasi-steadily, when the pitch rate is high, no quasi-steady behavior is observed. The dynamic pitching motion will always result in the delay of the vortex breakdown. The higher the pitch rate, the more effective the delay becomes. The trailing edge jet shows consistent large favorable effect during the transient pitching motion. It is very effective in slowing down the propagation of vortex breakdown location.

From the PIV study of the instantaneous cross-flow vorticity fields before vortex breakdown, quasi-periodic variation of the instantaneous vortical structures is observed. The variation of the instantaneous vortical structures is due to the interaction between the primary vortex and the secondary vortex. The distinct features of the instantaneous vortical structures can not be observed from the time-averaged vorticity field. This shows

that in order to have basic understanding of the delta wing flow field, instantaneous and whole-field measurement technique, such as PIV, is necessary.

5. REFERENCES

1. Rediniotis, O. K., Klute, S. M., Hoang, N. T., and Telionis, D. P. "**Dynamic Pitch-Up of a Delta Wing**", AIAA Journal, Vol. 32, No. 4, April 1994, pp. 716-725.

2. Polhamus, E. "**A Concept of the Vortex Lift on Sharp-Edge Delta Wings Based on a Leading Edge Suction Analogy**", NASA TN D-3767, December 1966.

3. Verhaagen, N. G., Kruisbrink, A.C.H. "**Entrainment Effect of a Leading-Edge Vortex**", AIAA Journal, August 1987, pp. 1025-1032.

4. Leibovich, S. "**Vortex Stability and Breakdown: Survey and Extension**", AIAA Journal, Vol. 22, No.9, September, 1984, pp. 1192-1206.

5. Lambourne, N. C., Bryer, D. W. "**The Bursting of Leading Edge Vortices; Some Observations and Discussion of the Phenomenon**", Aeronautical Research Council, R&M 3282, 1961.

6. Erickson, G. E. "**Effect of Spanwise Blowing on the Aerodynamic Characteristics of a Half-Span 50°-Swept Cropped Delta Wing Configuration**," AIAA Paper 79-1859, August, 1979.

7. Wentz, W. H., and Kolhman, D. L., " **Vortex Breakdown on Slender Sharp-Edge Wings**," AIAA Paper, No. 69-778.

8. Kegelman, J. T. and Roos, F. W. " **The Flow Field of Bursting Vortices Over Moderately Swept Delta Wings**," AIAA Paper, No. 90-0599.

9. Panton, R. L., "**The Effect of a Contoured Apex on Vortex Breakdown**," AIAA Paper No. 89-0193.

10 Lowson, M. V., "**Visualization Measurements of Vortex Flows**," Journal of Aircraft, Vol. 28, No.5, 1991, pp. 320-327.

11. Craven, A. H. and Alexander, A. J., " **An Investigation of Vortex Breakdown at Mach 2**," The College of Aeronautics, Cranfield, CoA Note Aero 158.

12. Monnerie, B. and Werlé, H., " **Etude de l'écoulement Supersonique et Hypersonique Autour d'une aile élancée en Incidence**," AGARD CP-30.

13. Hall, M. G. " **Vortex Breakdown**", Annual Review of Fluid Mechanics, vol. 4, 1972, pp. 195-218.

14. Grusul, I. and Ho, C. M., "**Vortex Breakdown over Delta Wings in Unsteady Free Stream**", AIAA paper 93-0555.

15. Lee, M. and Ho, C. M. "**Lift Force of Delta Wings**," Applied Mechanics Reviews, Vol. 43, No.9, September 1990, pp. 209-221.

16. Brown, G. L. and Lopez, J. M. "**Axisymmetric Vortex Breakdown, Part 2. Physical Mechanisms**," Journal of Fluid Mechanics, Vol. 221, 1990, pp. 553-576.

17. Towfighi, J. "**Instantaneous Structure of Vortex Breakdown on a Delta Wing**," M.S. thesis, Dept. of Mechanical Engineering and Mechanics, Leigh University, 1992.

18. Rockwell, D., Magness, C., Robinson, O., Towfighi, J., Akin, O., Gu, W., and Corcoran, T., "**Instantaneous Structure of Unsteady Separated Flows via Particle Image Velocimetry**," Dept. of Mechanical Engineering and Mechanics, Lehigh Univ., PI-1 Rept., February 1992.

19.Visbal, M. " **Structure of Vortex Breakdown on a Pitching Delta Wing,**" AIAA Paper 93-0434, Jan. 1993.
20. Gad-el-Hak, M. and Blackwelder, R. F., "**The Discrete Vortices from a Delta Wing,**" AIAA Journal, Vol. 23, No. 6, 1985. pp. 961-962.
21. Brown, G. L., and Roshko, A., "**On Density Effects and Large Structure in Turbulent Mixing Layers,**" Journal of Fluid Mechanics, Vol.64, July 1974, pp. 775-816.
22. Rediniotis, O. K., Stapountzis, H., and Telionis, D. P., "**Periodic Vortex Shedding over Delta Wing,**" AIAA Journal, Vol. 31, No. 9, September, 1993, pp. 1555-1562.
23. Payne, F. M., Ng, T. T., Nelson, R. C., and Schiff, L. B., "**Visualization and Flow Surveys of the Leading Edge Vortex Structure on Delta wing Platforms,**" AIAA Paper 86-0330, Jan. 1986.
24. Lowson, M. V., "**The Three Dimensional Vortex Sheet Structure on Delta Wings,**" Fluid Dynamics of Three-Dimensional Turbulent Shear Flow and Transition, AGARD-cp-438, Cesme, Turkey, October 1988. pp. 11-1--11-16.
25. Thompson, S., Batill, S., and Nelson, R., "**The Separated Flow Field on a Slender Delta Wing Undergoing Transient Pitching Motions,**" AIAA Paper 89-0194, January 1989.
26. Jarrah, M. A. "**Low-Speed Wind-Tunnel Investigation of Flow about Delta Wing Oscillating in Pitch to Very High Angle of Attack,**" AIAA Paper 89-0295, January 1989.
27. Magness, C., Robinson, O., and Rockwell, D., "**Control of Leading Edge Vortices on a Delta Wing,**" AIAA Paper 89-0999, March, 1989.
28. Lemay, S. P., Batill, S. M., and Nelson, R. C., "**Vortex Dynamics on a Pitching Delta Wing,**" Journal of Aircraft, Vol. 27, No.2, 1990, pp. 131-138.
29. Rediniotis, O. K., Klute, S. M., Hoang, N. T., and Telionis D. P., "**Dynamic Pitching-up of a Delta wing,**" AIAA Journal, Vol. 32, No. 4, April 1994, pp. 716-725.
30. Erickson, G. E., and Campbell, J. F., "**Augmentation of Maneuver Performance by Spanwise Blowing,**" TM X-73998, NASA, December, 1977.
31. Werlé, H., "**Division and Coming Together of Fluid Flows,**" La Rech. Aeron., No.79, 1960.
32. Erickson, G. E., "**Experimental Investigation of the F/A-18 Vortex Flow at Subsonic Speed,**" AIAA Paper, 89-2222, 1989.
33. Bradley, R. G., Whitten, P. D., and Wray, W. O, "**Leading Edge Vortex Augmentation in Compressible Flow,**" Journal of aircraft, Vol. 13, No. 4, 1976, pp. 238-242.
34. Shi, Z., Wu, J. M., and Vakili, A. D. "**An Investigation of Leading Edge Vortices with Jet Blowing,**" AIAA Paper 87-0330, January 1987.
35. Wood, N. J., and Roberts, L., "**The Control of Vortical Lift on Delta Wings by Tangential Leading Edge Blowing,**" AIAA Paper 87-0158, January 1987.
36. Gu, W., Robinson, O., and Rockwell, D. "**Control of Vortices on a Delta Wing by Leading Edge Injection,**" AIAA Journal, Vol. 31, No. 7, July 1993.
37. Srinivas, S., Grusul, I., and Batta, G., "**Active Control of Vortex Breakdown over Delta Wings,**" AIAA Paper 94-2215.

38. Hagedorn, H. and Ruden, P., Lilienthal-Gesellschaft Bericht, A 64, 1938
39. Bower, D. L., "**Aerodynamic Effects Induced by a Vectored High Aspect Ratio Non-axisymmtric Exhaust Nozzle**," Journal of Aircraft, Vol. 16, August, 1979.
40. Schnell, W. C., and Grossman, R. L., "**Vectoring Nonaxisymmetric Nozzle Jet Induced Effects on a V/STOL Fighter Model**," Journal of Aircraft, Vol. 16, December, 1979.
41. Paulson, J. W., "**Analysis of Thrust-Induced Effects on the Longitudinal Aerodynamics of STOL Fighter Configurations**," Journal of Aircraft, Vol.18, November, 1981.
42. Adrian, R. J., "**Particle Imaging Techniques for Experimental Fluid Mechanics**," Annual Review of Fluid Mechanics, Vol. 23, 1991, pp. 261-304.
43. Lourenco, L., Krothipalli, A., and Smith, C., "**Particle Image Velocimetry**," Lecture Notes in Engineering 45, Advances in Fluid Mechanics Measurements, ed. Gad-el-Hak, Spring-Verlog, 1989, pp. 127-199.
44. Adrian, R. J., "**An Image Shifting Technique to Resolve Directional Ambiguity in Double Pulsed Laser Velocimetry**," Applied Optics, Vol. 25, 1986, pp. 3855-3858.
45. Lourenco. L. "**A Passive Velocity Bias Technique for PIDV**," Bulletin of American Physics Society, Vol. 34, 1989, p.2267.
46.Lourenco. L. and Krothipalli, A., "**The Role of Photographic Parameters in Laser Speckle or Particle Image Displacement Velocimetry**," Experiments in Fluids, 5, 1987, pp. 29-32.
47. Helin, H. E., and Watry, C. W., "**Effects of Trailing Edge Jet Entrainment on Delta Wing Vortices**," AIAA Journal, vol. 32, No.4, April 1994, pp. 802-804.

APPENDIX I: FIGURES

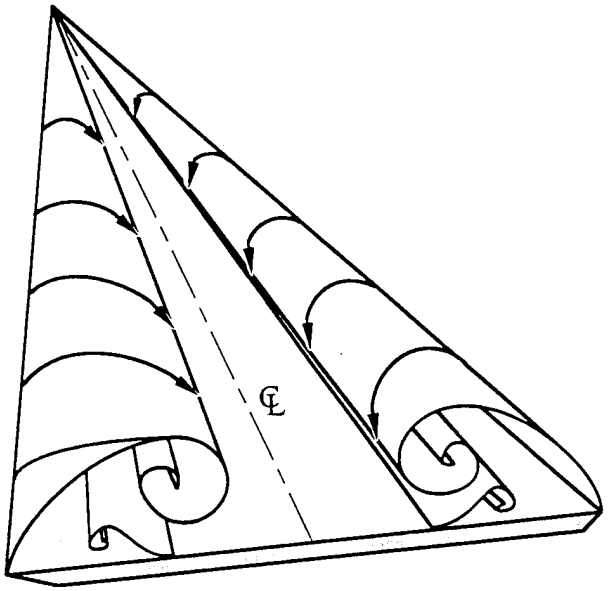

Figure 1 Sketch of delta wing leading edge vortex

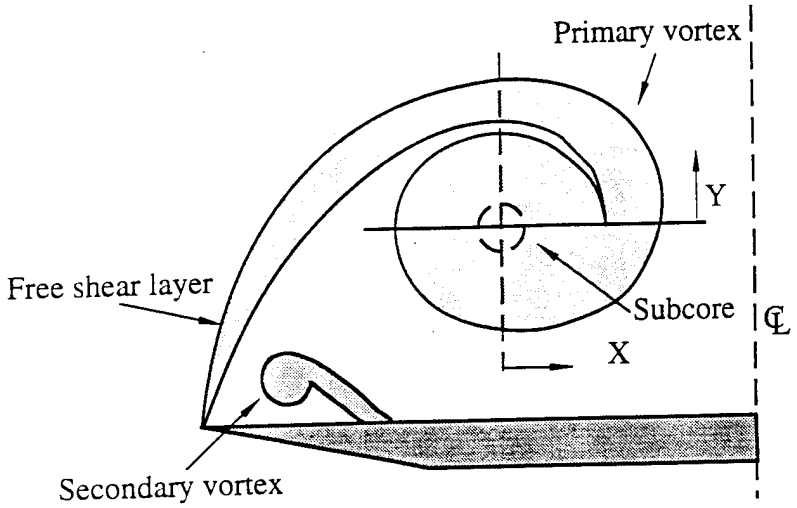

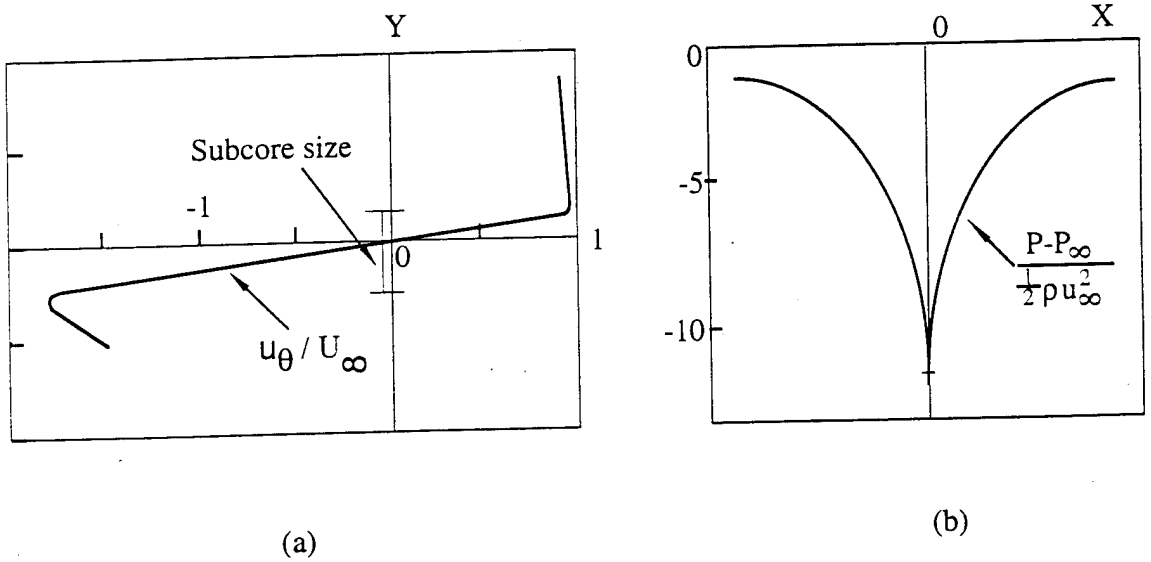

(a) (b)

Figure 2 Sketch of the cross-sectional leading edge vortex and the distribution of (a) circumferencial velocity (b) static pressure

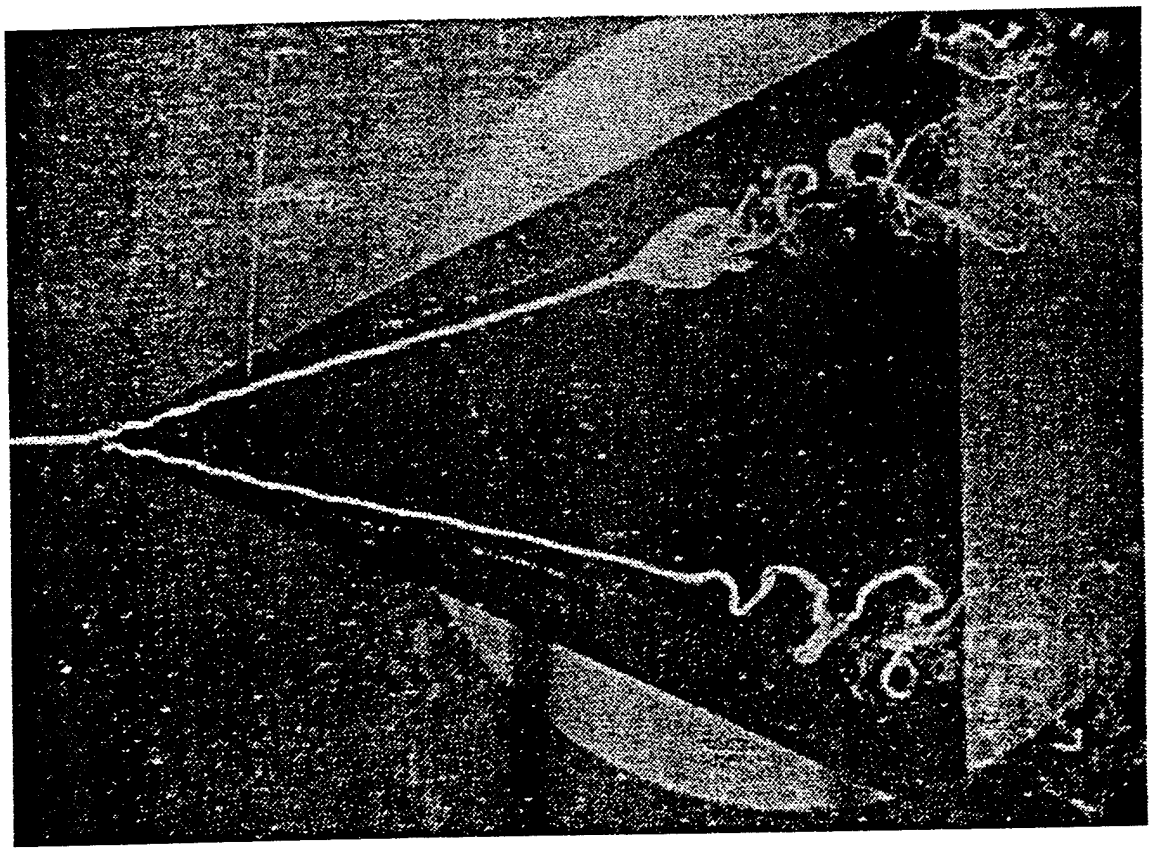

Figure 3 Two types of vortex breakdown over delta wing, The upper one is a bubble type; the lower one is a spiral type.

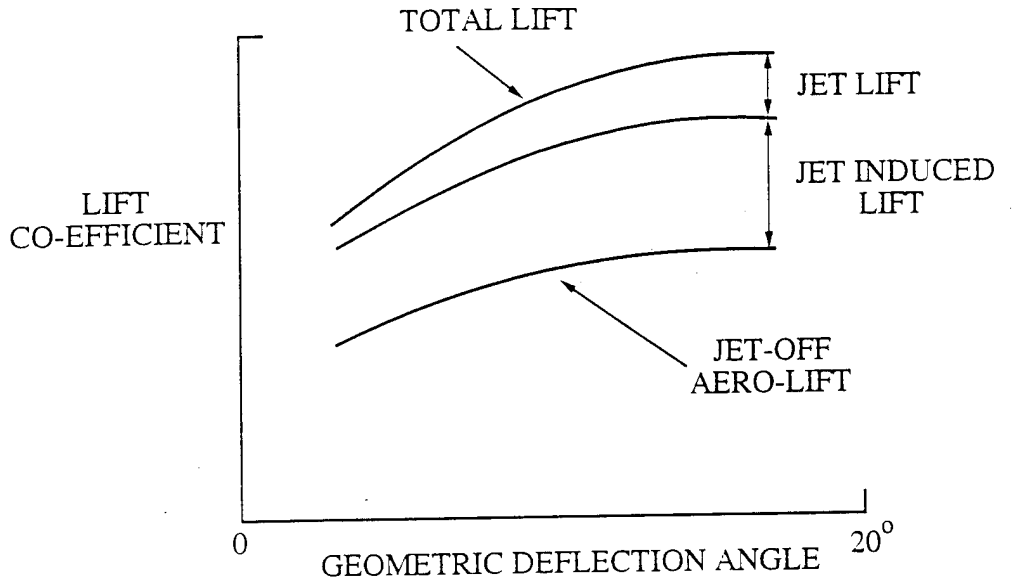

(a)

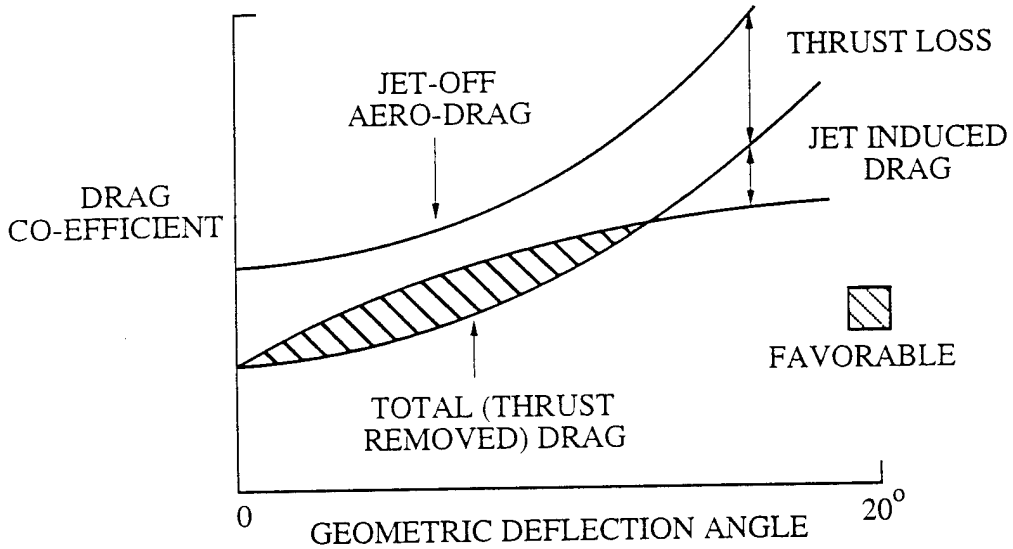

(b)

Figure 4 Thrust-induced effect on the aerodynamics of the aircraft (a) induced lift due to thrust-vectoring (b) reduced drag due to thrust recovery

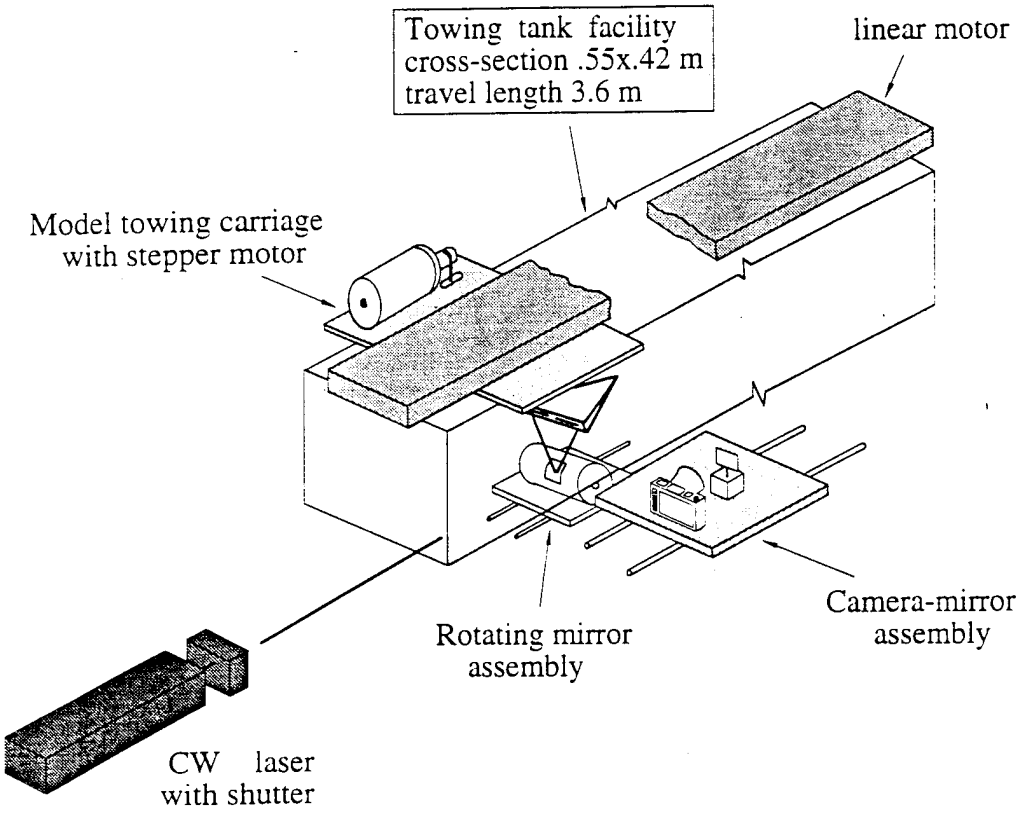

Figure 5 Water Towing tank facility and PIV photographic arrangement

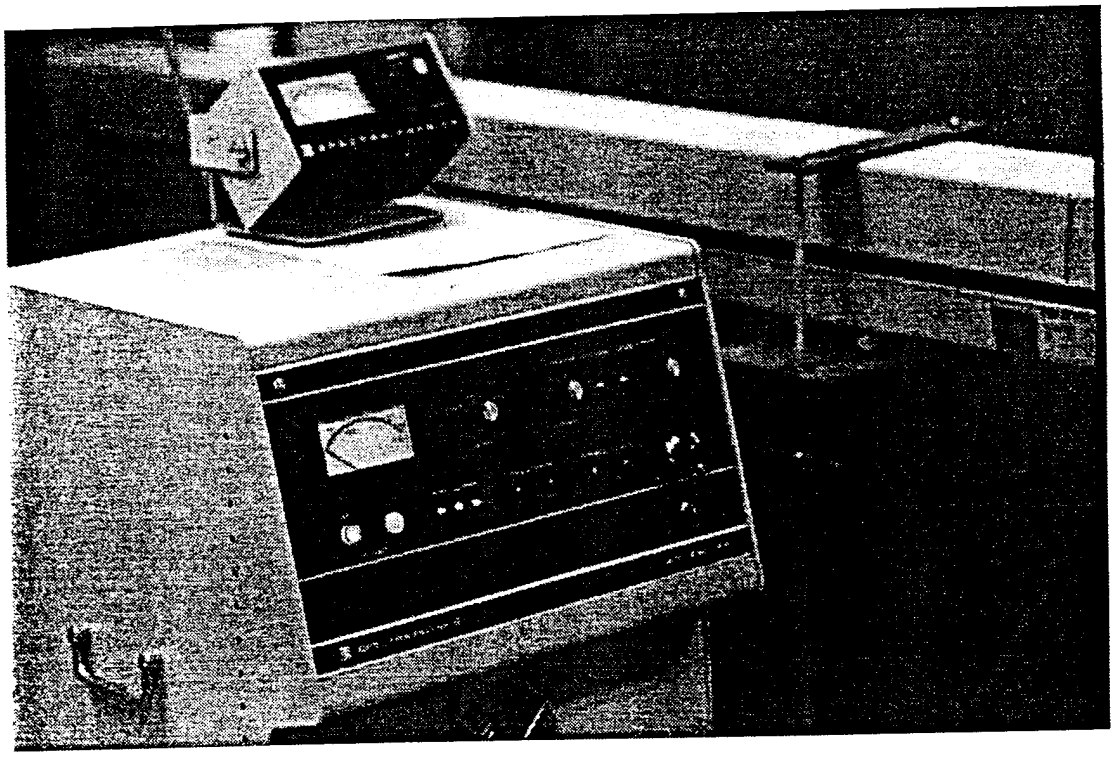

Figure 6 Argon-Ion Laser

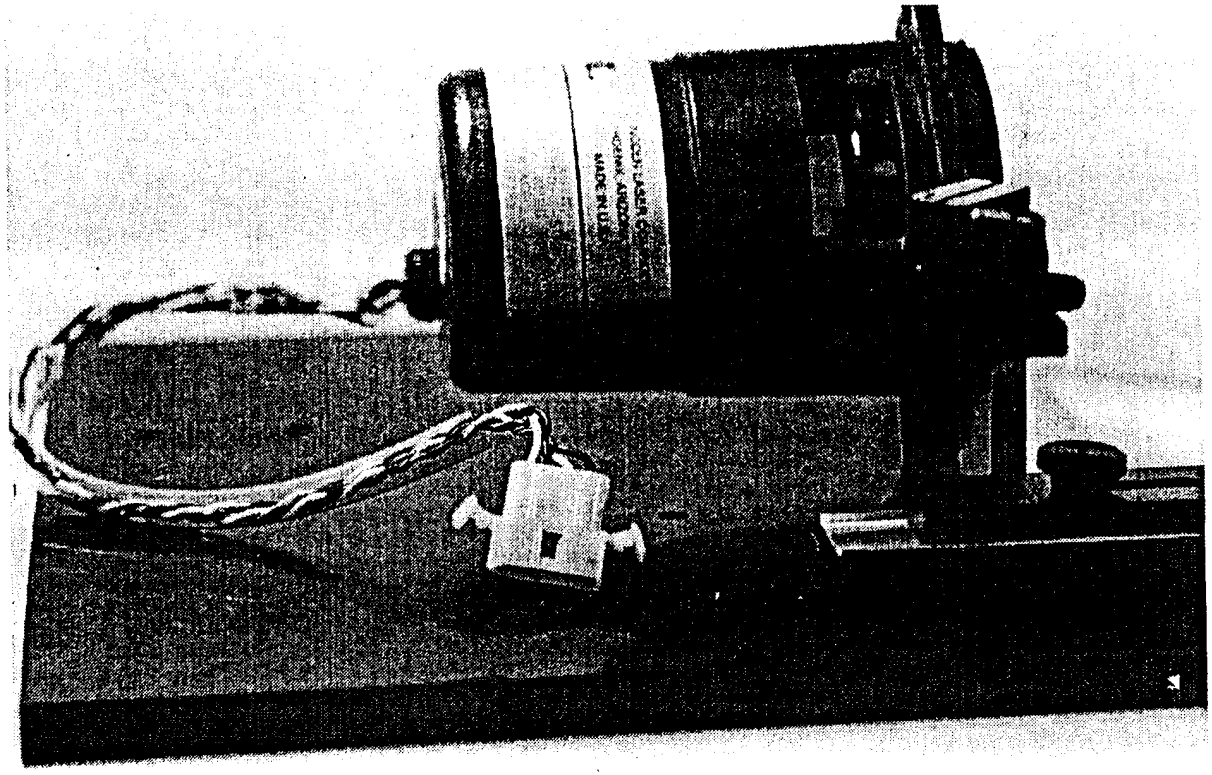

Figure 7 24-faceted spinning mirror

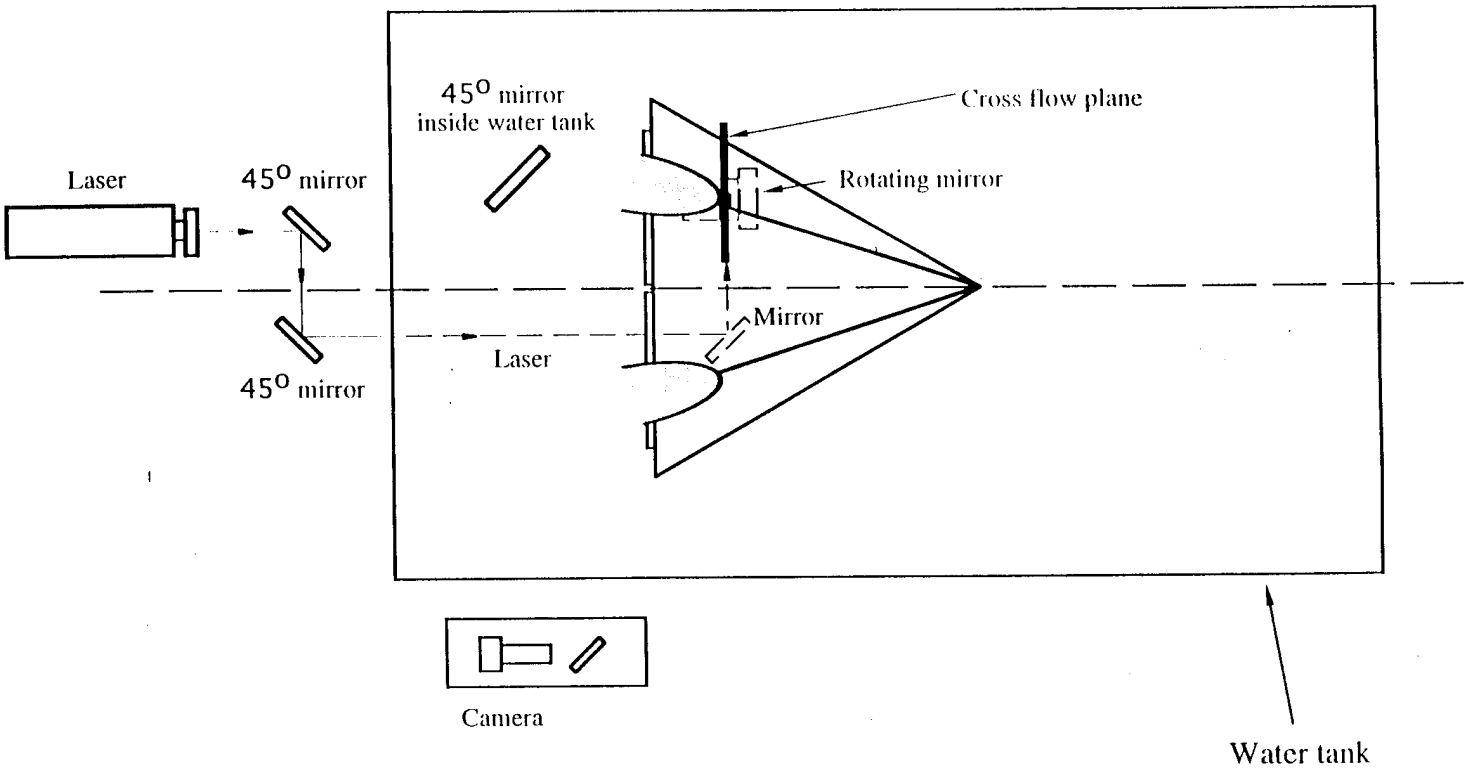

Figure 8 PIV setup for the cross-flow plane

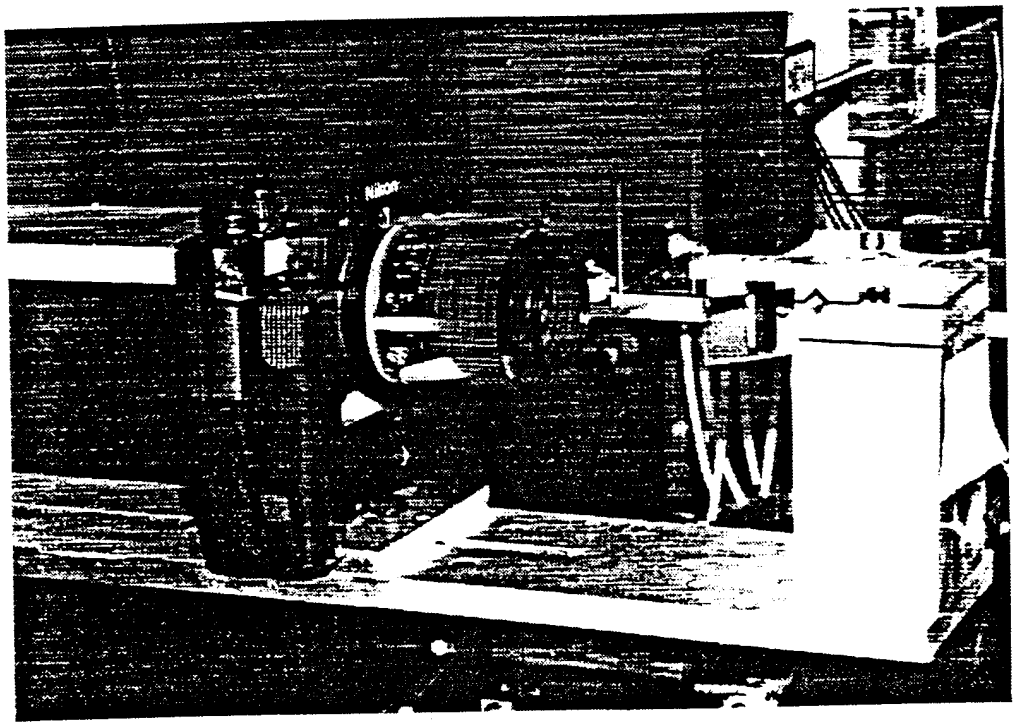

Figure 9 Image recording system

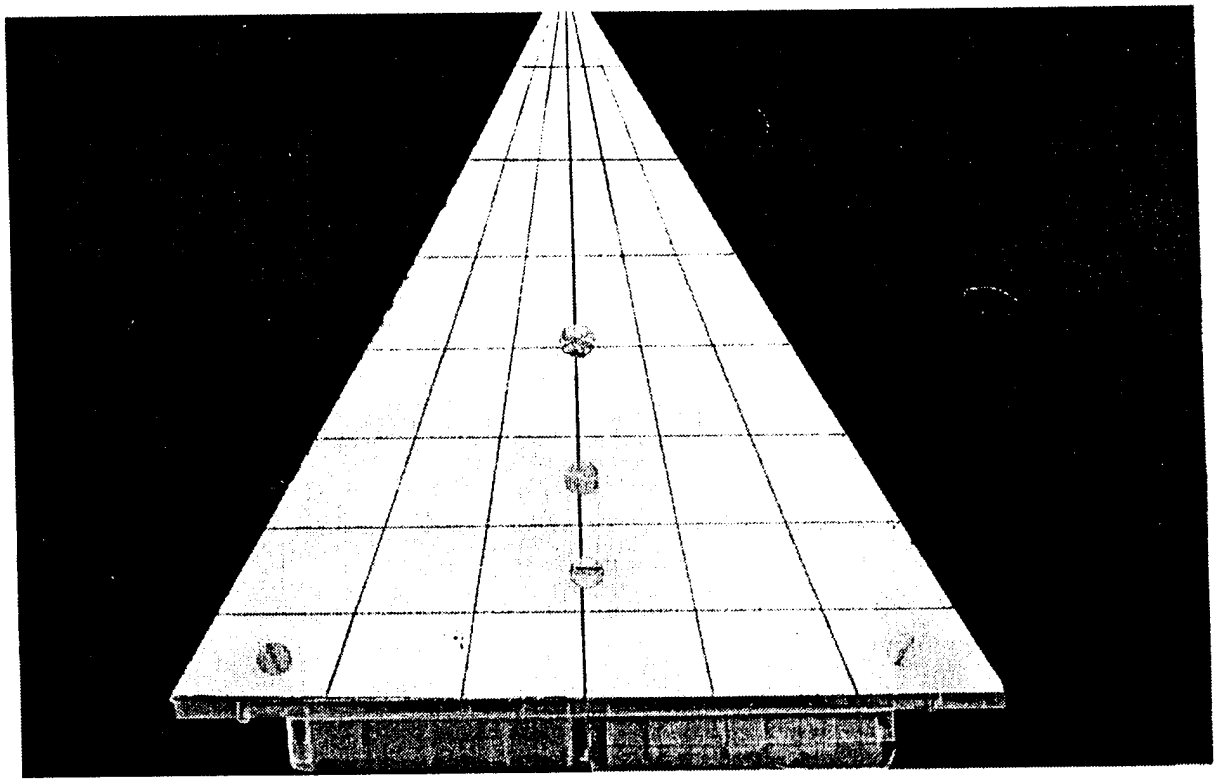

Figure 10 Top view of the delta wing

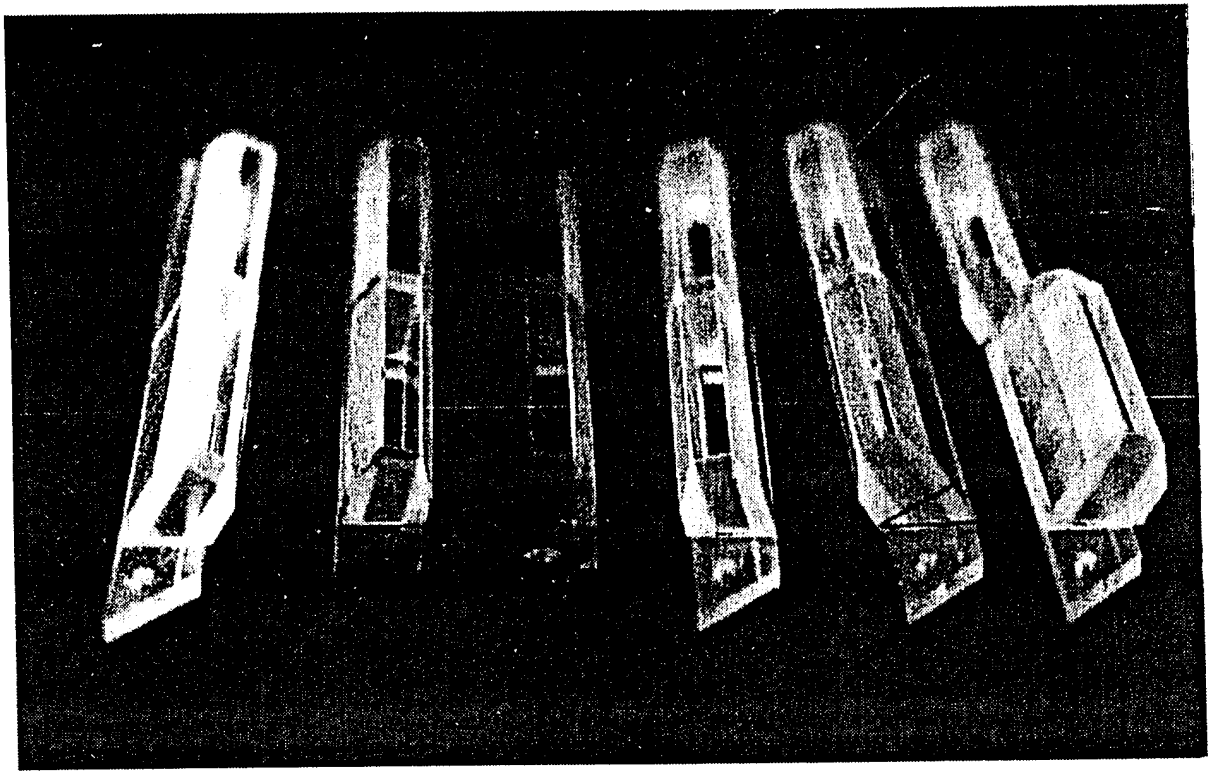

Figure 11 Different trailing edge nozzles. From left to right: symmetric: 30° and 15° downward, 0°, 15° and 30° upward, asymmetric: one 30° down and one 30° upward.

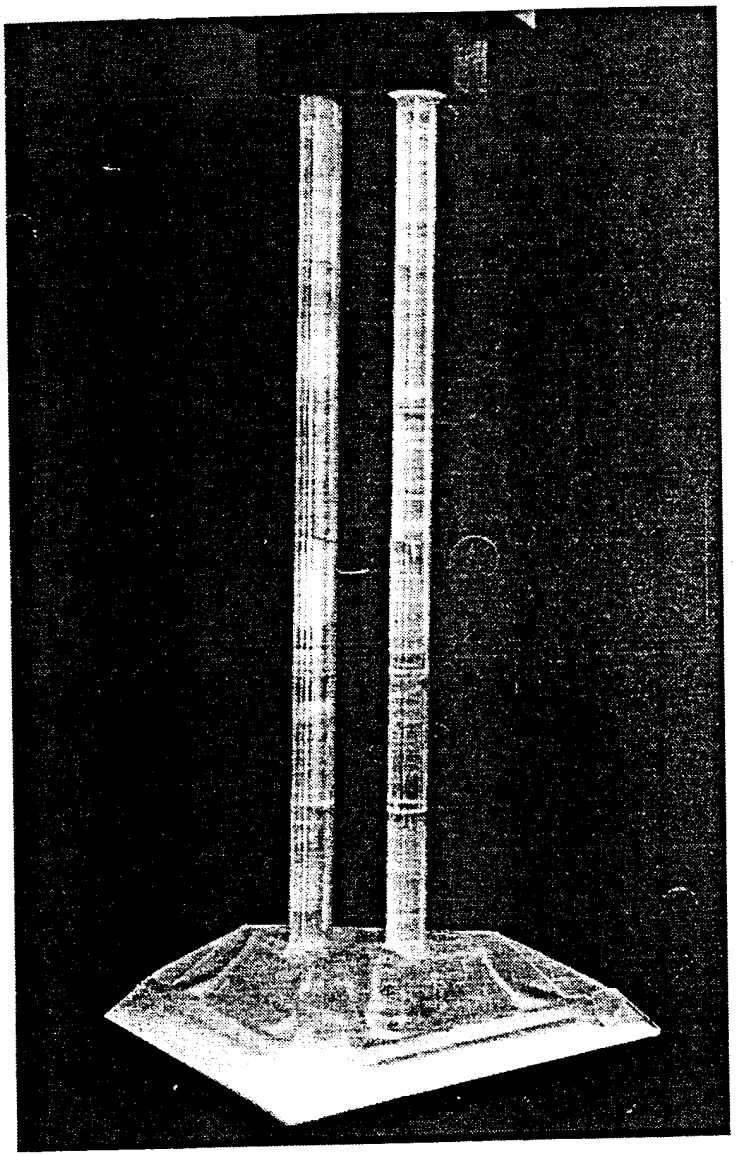

Figure 12 Sting support of the delta wing

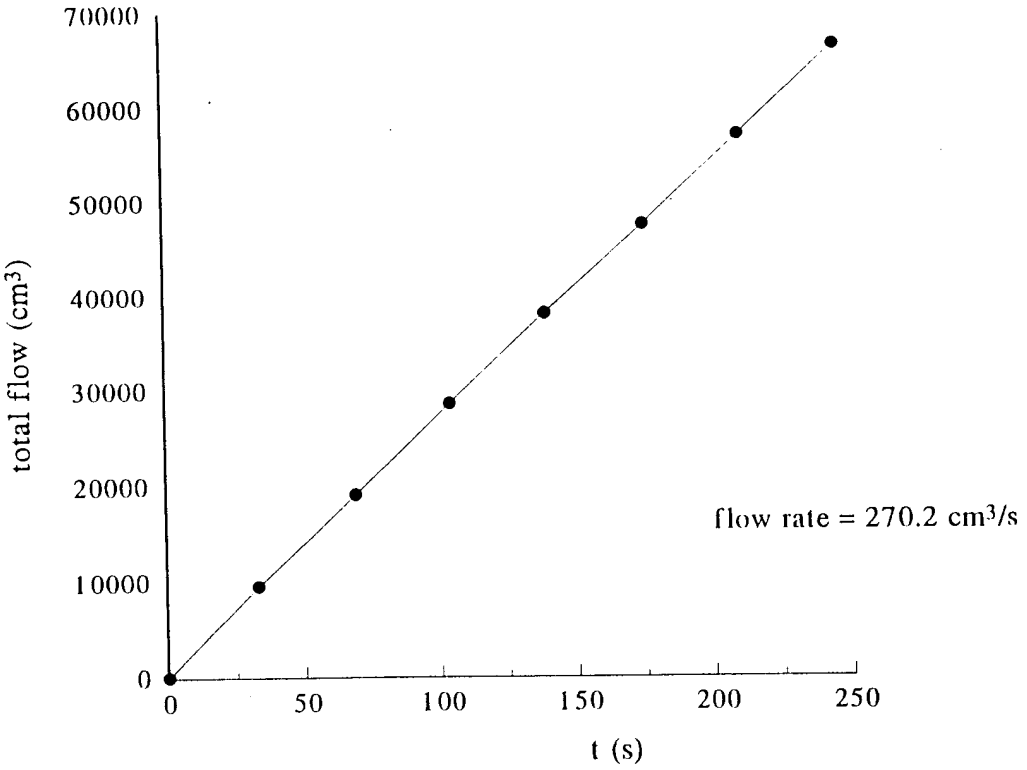

Figure 13 Calibration of the trailing edge jet flow rate

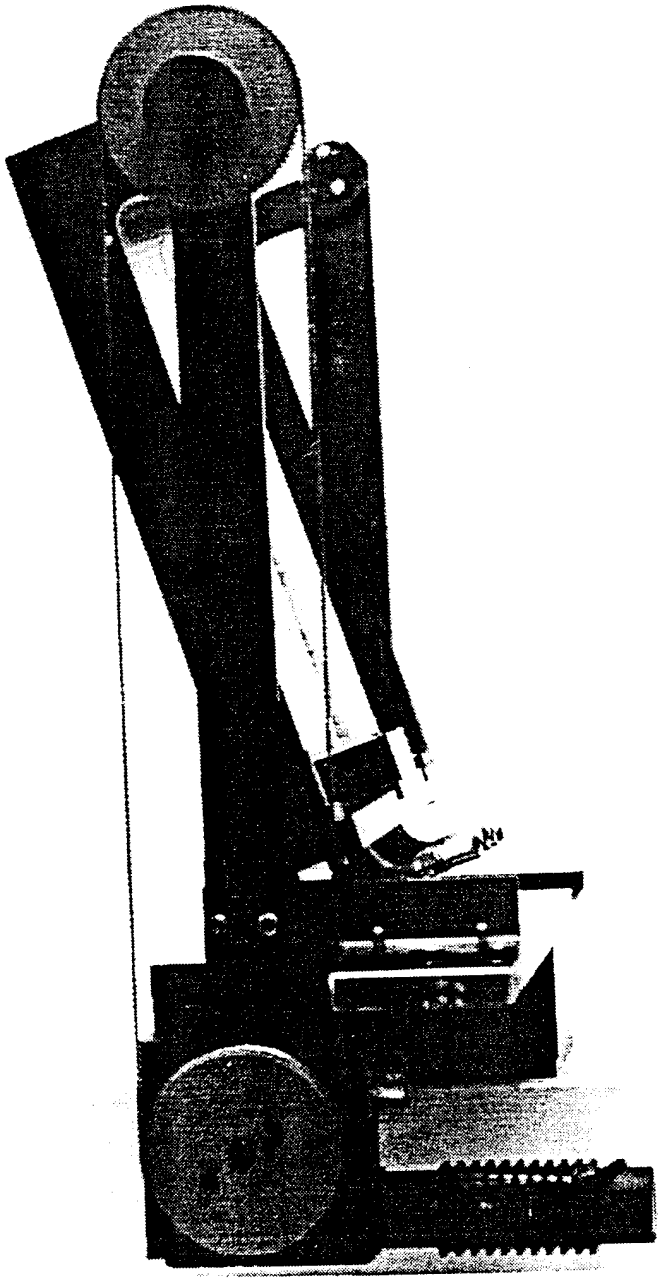

Figure 14 Pitching mechanism of the delta wing
(a) side view

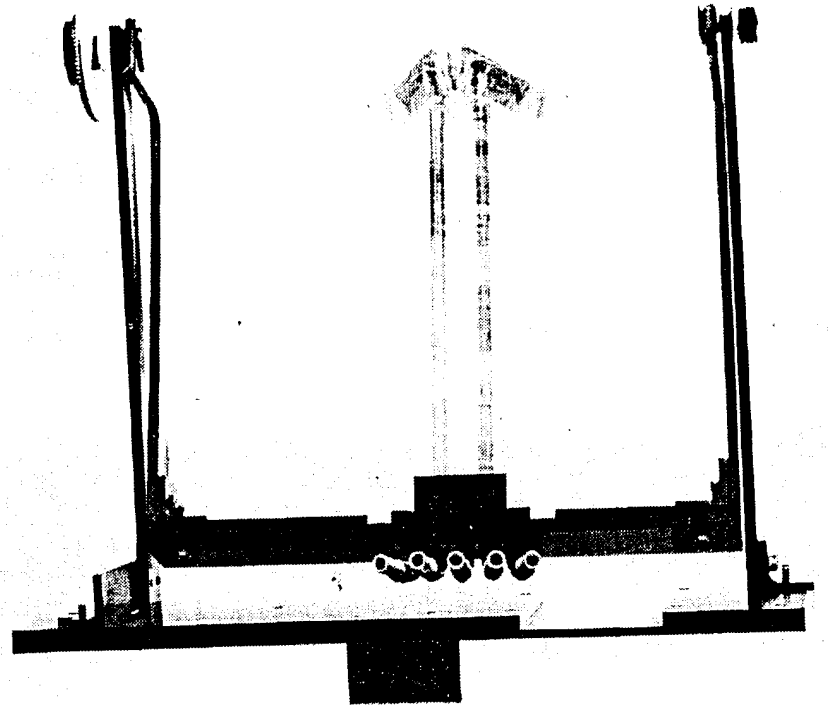

Figure 14 Pitch mechanism of the delta wing
(b) front view

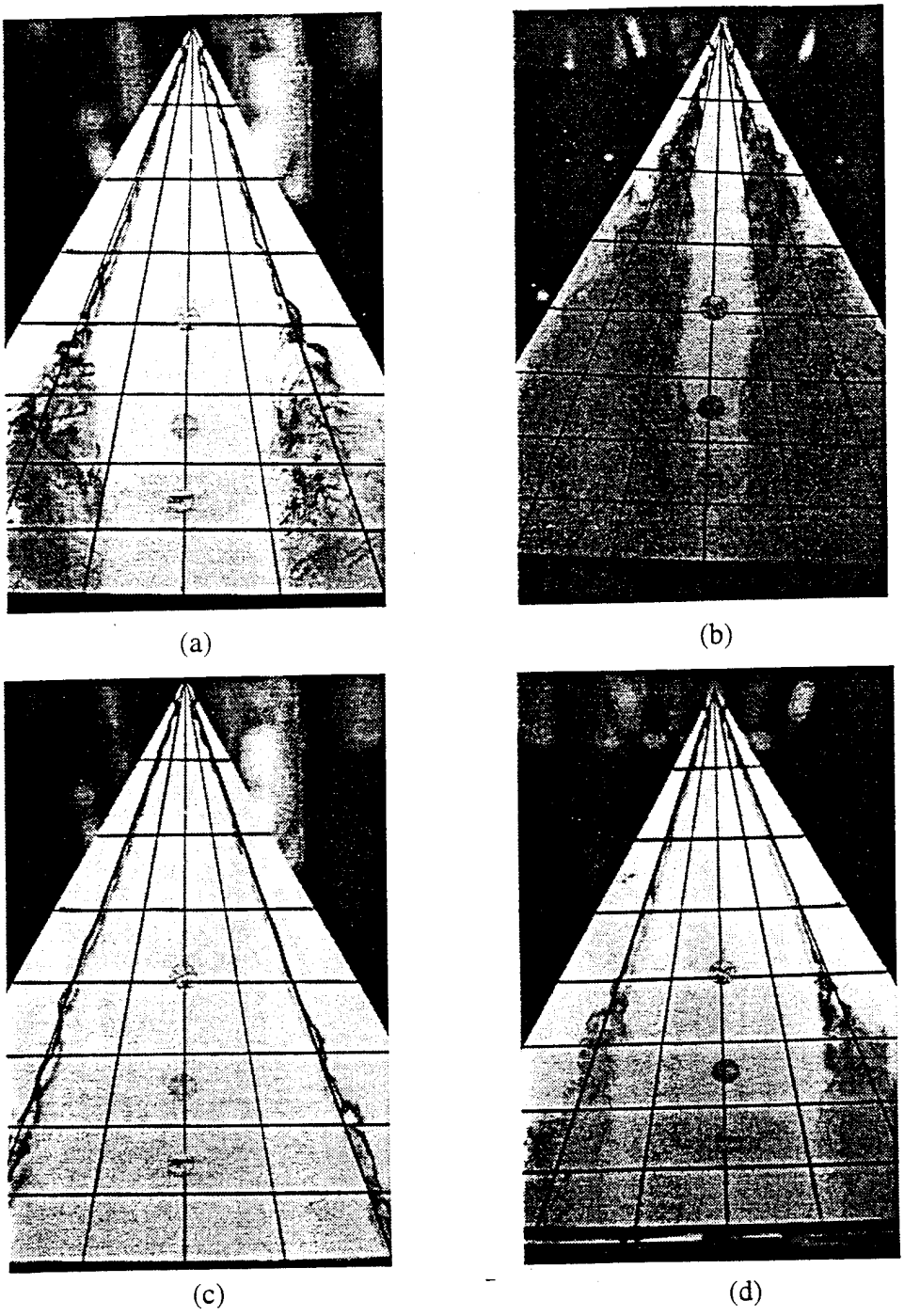

Figure 15 Flow visulization results of a static delta wing.
no control: (a) AOA=15°, (b) AOA=25°; with 45°
downward jet control: (c) AOA=15°, (d) AOA=25°

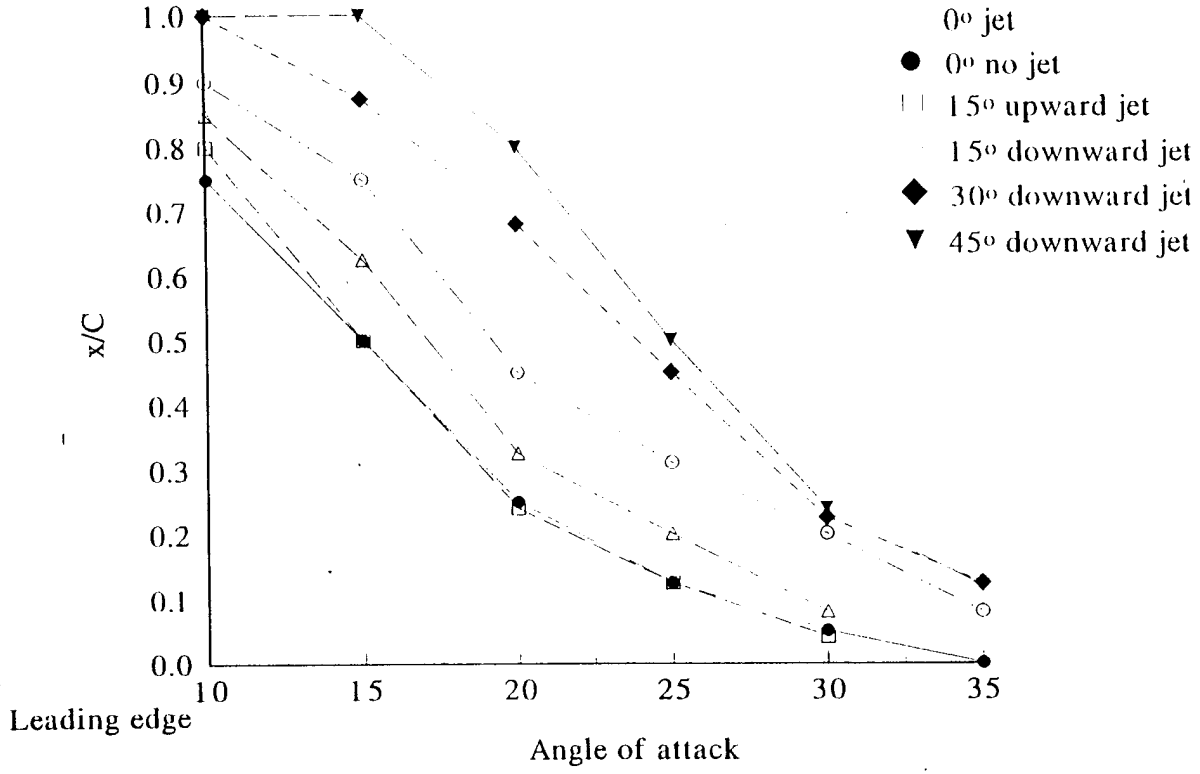

Figure 16 Breakdown location vs. angle of attack, static case, with symmetric trailing edge jet control

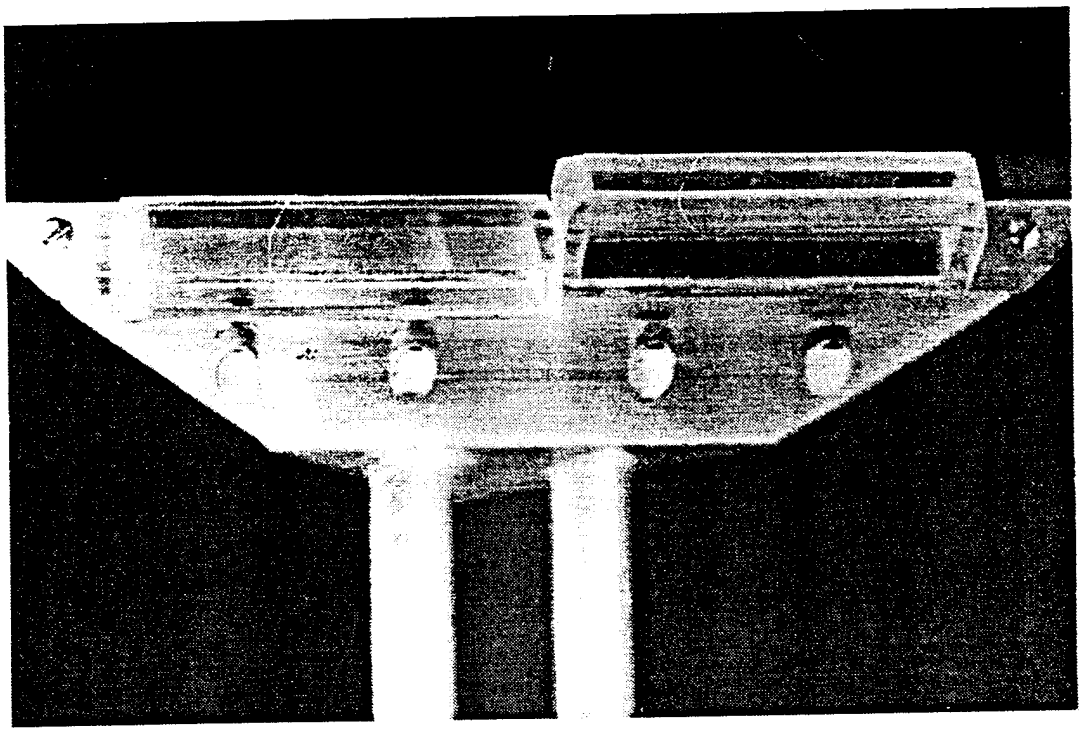

Figure 17 Asymmetric trailing edge control jet nozzles

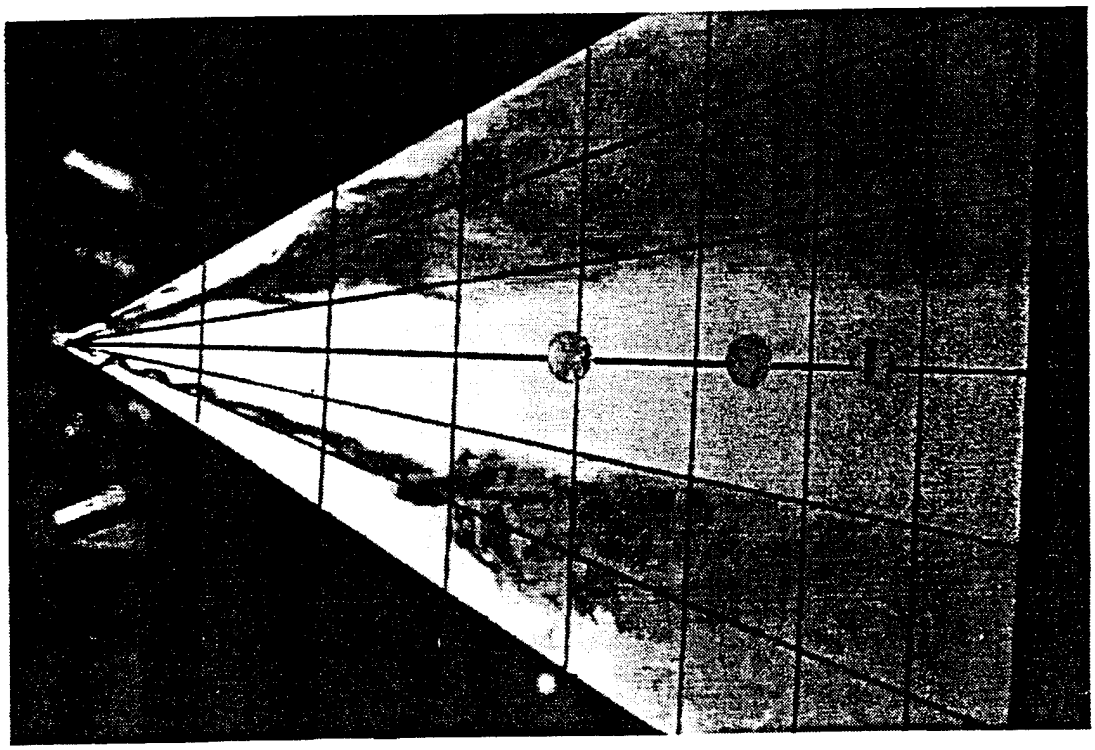

Figure 18 Flow visulization result of a static delta wing, asymmetric trailing edge jet control, $\alpha = 25^{o}$

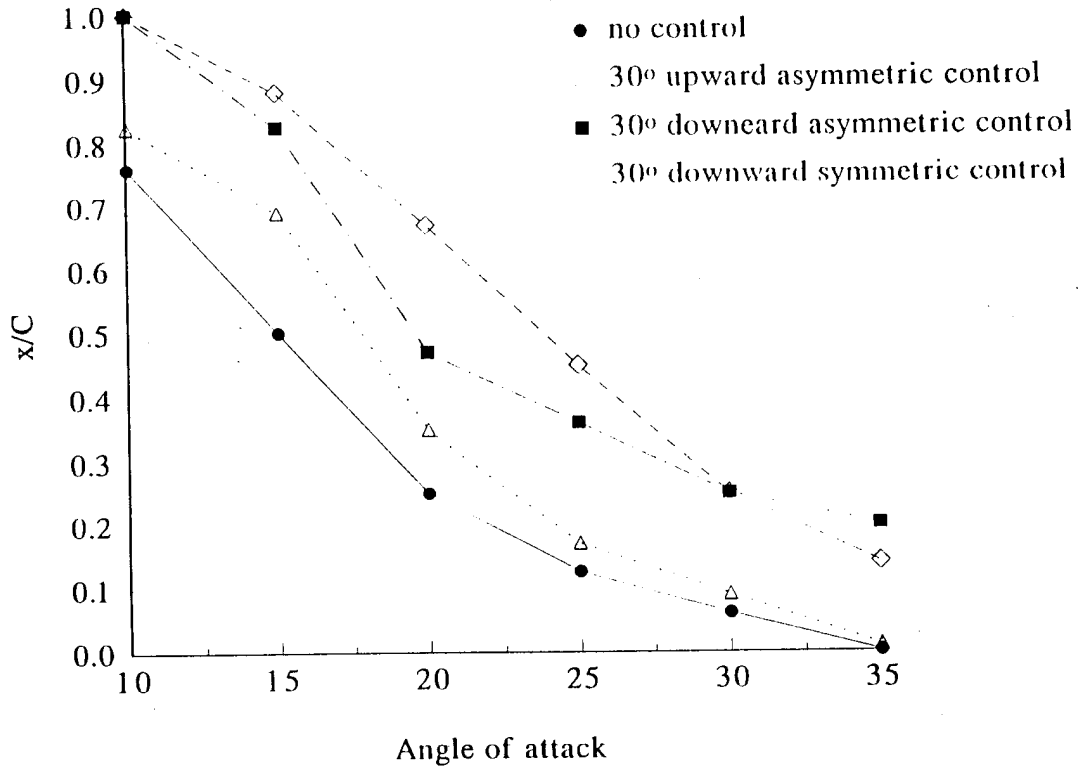

Figure 19 Vortex breakdown location vs. static angle of attack

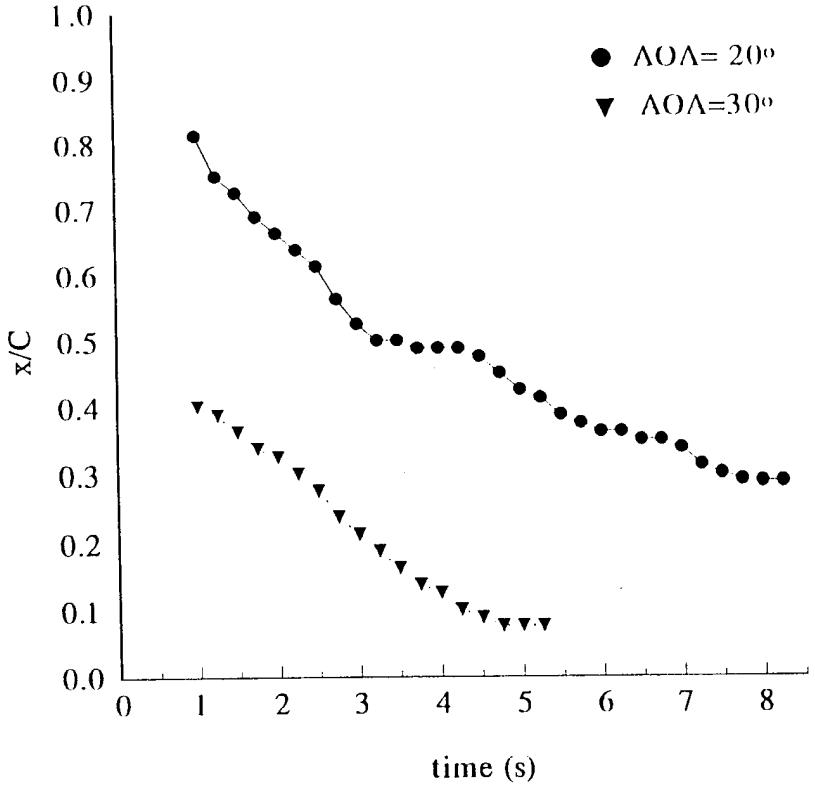

Figure 20 Effect of impulsive start on leading edge vortex flow

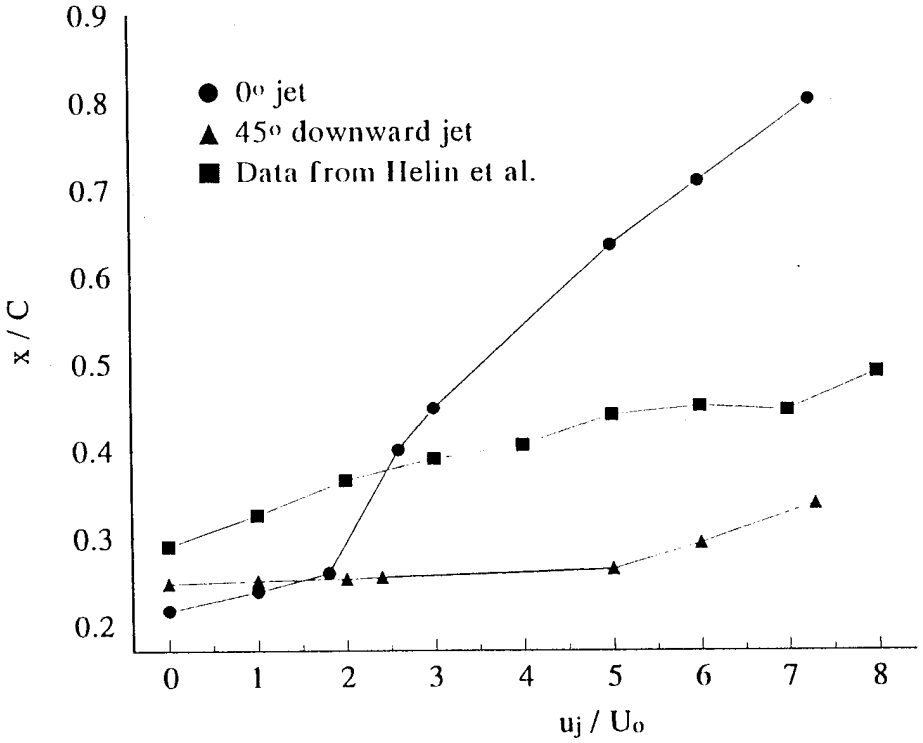

Figure 21 Effect of trailing edge jet velocity on vortex breakdown

AOA=20°

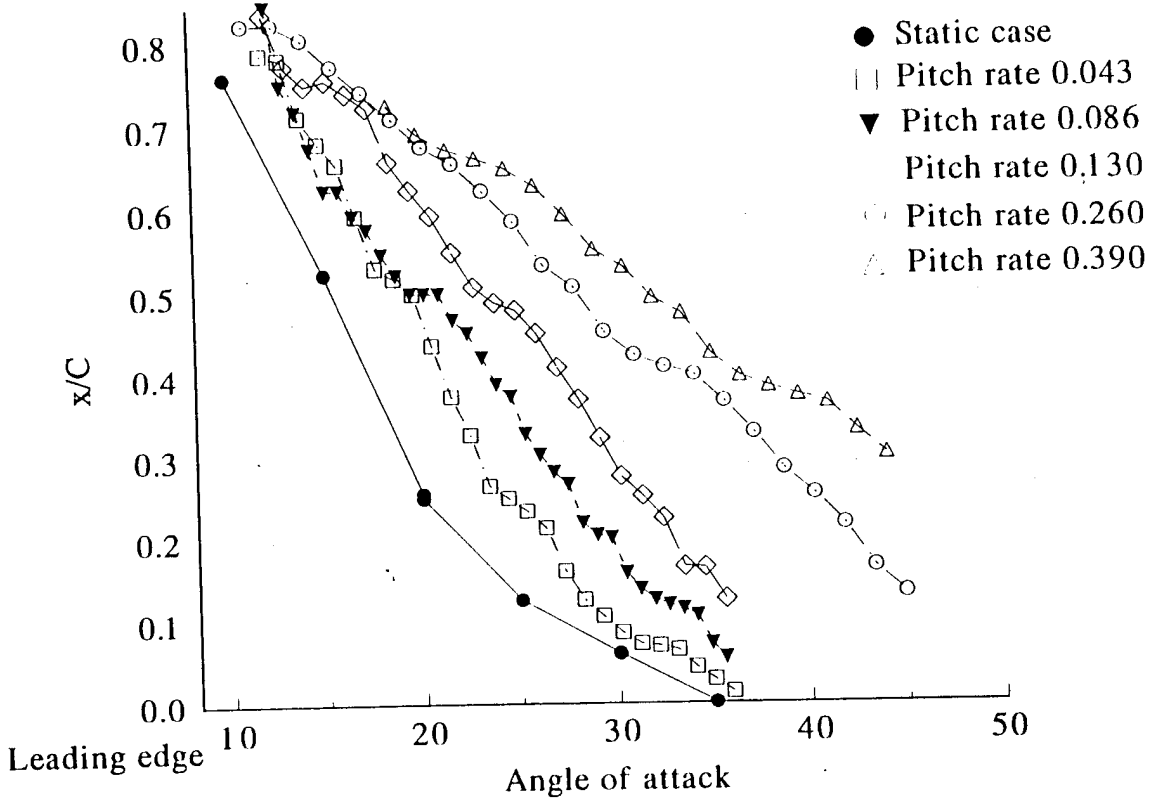

Figure 22 Breakdown location vs. the angle of attack, no control, with different pitch rate

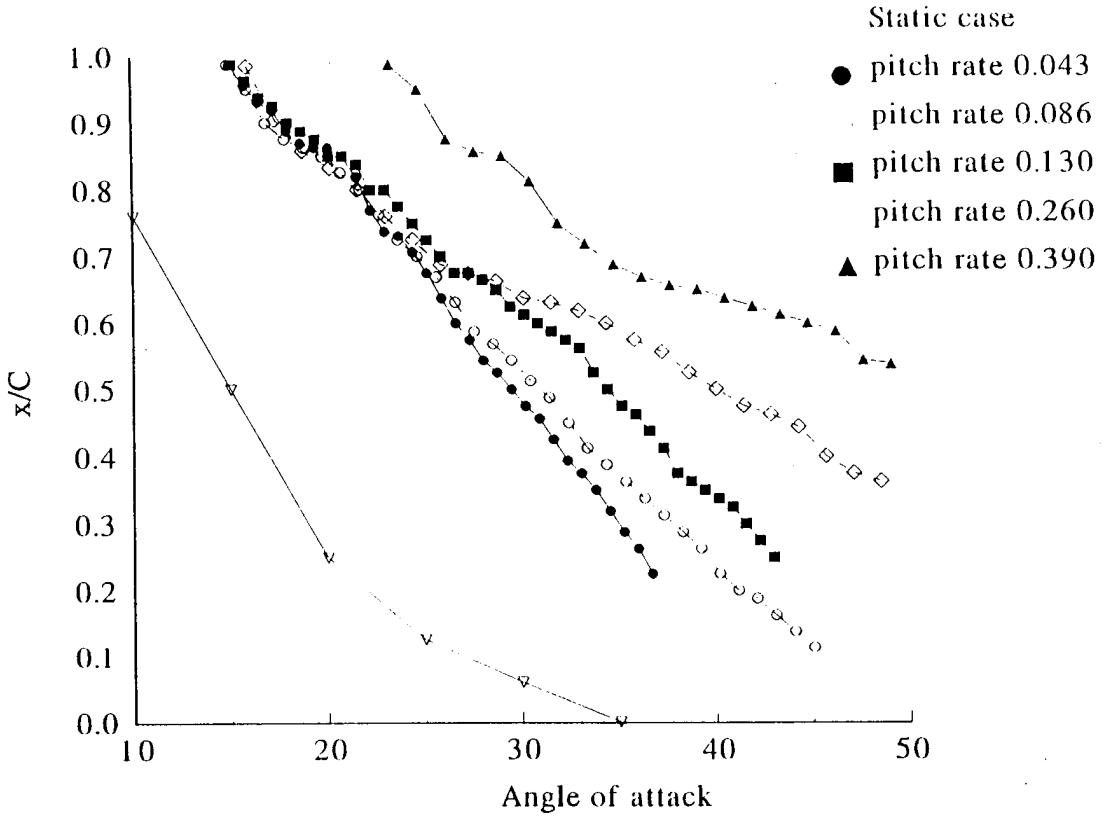

Figure 23 Vortex breakdown location vs. the angle of attack with 45° trailing edge jet control

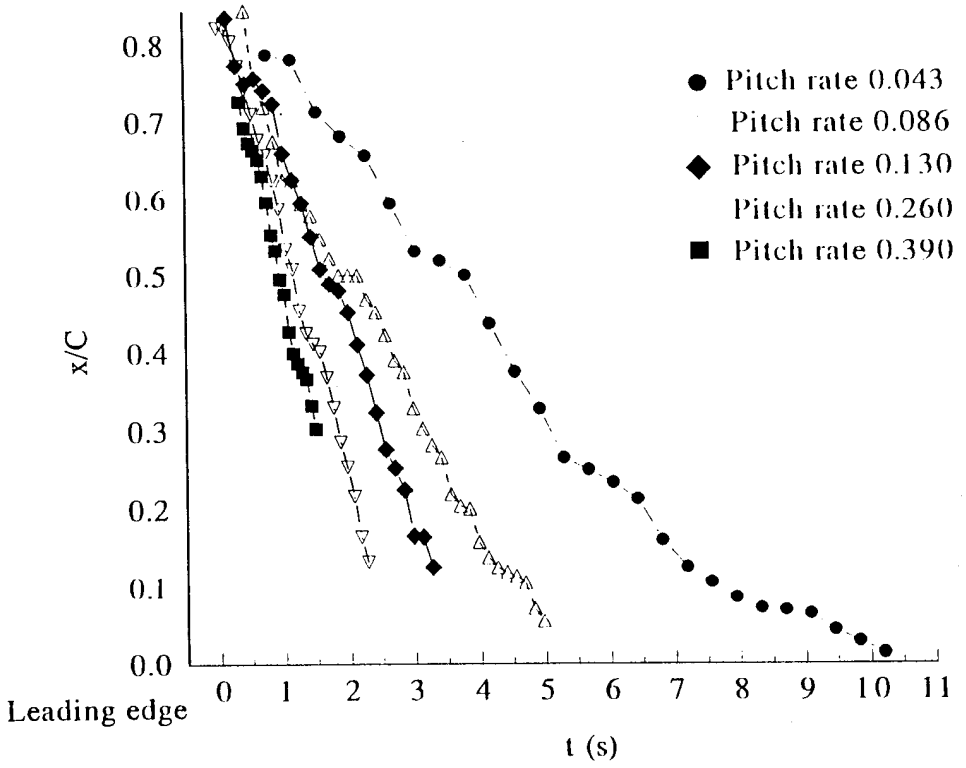

Figure 24 Breakdown location vs. the time
no control, with different pitch rate

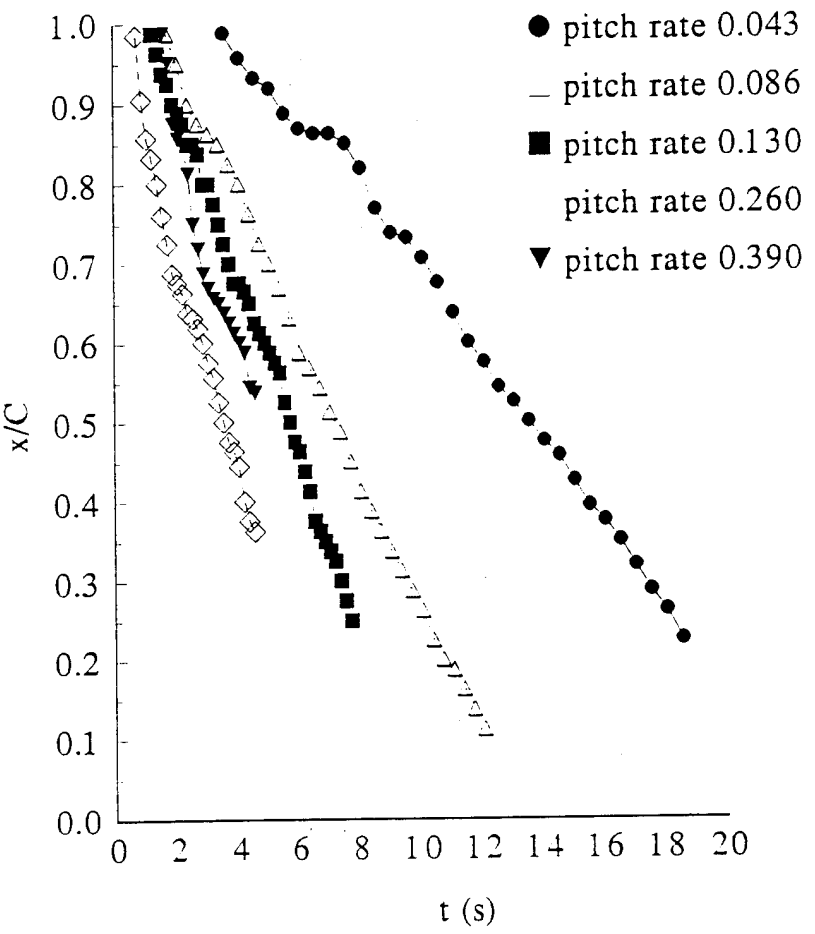

Figure 25 Vortex breakdown location vs. time with 45° downward trailing edge jet control